NASA CONTRACTOR
REPORT

NASA CR-1887

NASA CR

C. 1

BUCKLING ANALYSIS FOR AXIALLY COMPRESSED FLAT PLATES, STRUCTURAL SECTIONS, AND STIFFENED PLATES REINFORCED WITH LAMINATED COMPOSITES

*by A. V. Viswanathan, Tsai-Chen Soong,
and R. E. Miller, Jr.*

Prepared by
THE BOEING COMPANY
Seattle, Wash. 98124
for Langley Research Center

NATIONAL AERONAUTICS AND SPACE ADMINISTRATION • WASHINGTON, D. C. • NOVEMBER 1971

1. Report No. NASA CR-1887	2. Government Accession No.	3. Recipient's Catalog No.
4. Title and Subtitle BUCKLING ANALYSIS FOR AXIALLY COMPRESSED FLAT PLATES, STRUCTURAL SECTIONS, AND STIFFENED PLATES REINFORCED WITH LAMINATED COMPOSITES		5. Report Date November 1971
		6. Performing Organization Code
7. Author(s) A. V. Viswanathan, Tsai-Chen Soong, and R. E. Miller, Jr.		8. Performing Organization Report No.
9. Performing Organization Name and Address The Boeing Company Commercial Airplane Group Seattle, Washington 98124		10. Work Unit No. 126-14-17-01
		11. Contract or Grant No. NASI-8858
12. Sponsoring Agency Name and Address Langley Research Center Hampton, Va. 23365		13. Type of Report and Period Covered Contractor Report
		14. Sponsoring Agency Code

15. Supplementary Notes

16. Abstract

A classical buckling analysis is developed for stiffened, flat plates composed of a series of linked flat plate and beam elements. Plates are idealized as multilayered orthotropic elements, structural beads and lips are idealized as beams. The loaded edges of the stiffened plate are simply supported and the conditions at the unloaded edges can be prescribed arbitrarily. The plate and beam elements are matched along their common junctions for displacement continuity and force equilibrium in an exact manner. Offsets between elements are considered in the analysis. Buckling under uniaxial compressive load for plates, sections and stiffened plates is investigated. Buckling loads are found as the lowest of all possible general and local failure modes and the mode shape is used to determine whether buckling is a local or general instability. Numerical correlations with existing analysis and test data for plates, sections and stiffened plates including boron-reinforced structures are discussed. In general, correlations are reasonably good.

17. Key Words (Suggested by Author(s)) Buckling, Compression, Stiffened Plate, Composite, Fiber-Reinforced, Stability, Plate	18. Distribution Statement Unclassified - Unlimited

19. Security Classif. (of this report) Unclassified	20. Security Classif. (of this page) Unclassified	21. No. of Pages 79	22. Price* $3.00

TABLE OF CONTENTS

LIST OF FIGURES

LIST OF TABLES

BUCKLING ANALYSIS FOR AXIALLY COMPRESSED FLAT PLATES,

STRUCTURAL SECTIONS, AND STIFFENED PLATES REINFORCED

WITH LAMINATED COMPOSITES

by

A. V. Viswanathan, Tsai-Chen Soong, R. E. Miller, Jr.

The Boeing Company, Seattle, Washington

1. ABSTRACT

A classical buckling analysis is developed for stiffened, flat plates composed of a series of linked flat plate and beam elements. Plates are idealized as multilayered orthotropic elements; structural beads and lips are idealized as beams. The loaded edges of the stiffened plate are simply supported and the conditions at the unloaded edges can be prescribed arbitrarily. The plate and beam elements are matched along their common junctions for displacement continuity and force equilibrium in an exact manner. Offsets between elements are considered in the analysis. Buckling under uniaxial compressive load for plates, sections and stiffened plates is investigated. Buckling loads are found as the lowest of all possible general and local failure modes and the mode shape is used to determine whether buckling is a local or general instability. Numerical correlations with existing analysis and test data for plates, sections and stiffened plates including boron-reinforced structures are discussed. In general, correlations are reasonably good.

1

2. NOMENCLATURE

a	length of plate, Eq. (5.1)
$A_{11}, A_{12}, A_{22}, A_{66}$	matrix elements, Eq. (4.7)
A_b	cross sectional area of beam
b	width of plate, Eq. (5.1)
$B_{11}, B_{12}, B_{22}, B_{66}$	elements of matrix, Eq. (4.8)
$D_{11}, D_{12}, D_{22}, D_{66}$	elements of matrix, Eq. (4.9)
$E_{11}, E_{22}, G_{12}, G_{23}$	orthotropic modulus of elasticity, Eq. (4.2)
$G_{1i}, G_{2i}, G_{3i}, G_{4i}$	Eqs. (5.10a)
h_k	distance of the kth layer to the reference plane, Fig. 4.1
h_k'	distance of kth layer to the neutral plane, Fig. 4.1
I	moment of inertia
I_{xx}, I_{yy}, I_{zz}	moment of inertias of beam about x, y and z axes, Fig. 4.2
J	torsional constant, Eq. (4.12)
$\lceil k_{RG} \rfloor$	diagonal matrix for spring constants, Eq. (5.57)
$k_{UG}, k_{VG}, k_{WG}, k_{\theta G}$	spring constants in the global coordinate directions, Eq. (5.57)
k_x, k_θ, k_u, k_v	spring constants, Eqs. (5.2) and (5.3)
$K_8, K_6, \ldots K_0$	coefficients of characteristic equation, Eq. (5.6)
ℓ	total number of layers of a laminated plate, Eq. (4.3)
L_{1i}, L_{2i}	Eqs. (5.8)
m	half-wave number, Eq. (5.1)
$(m_{22})_i$	Eq. (5.20)
M_{11}, M_{12}, M_{22}	moments, Eq. (4.6)
$(n_{12})_i$	Eq. (5.21)
$(n_{22})_i$	Eq. (5.22)
N_{11}, N_{22}, N_{12}	stress resultants, Eq. (4.5)
$\bar{N}_{11}, \bar{N}_{22}, \bar{N}_{12}$	in-plane buckling loads, lb/in., Eq. (4.16)
p_i	parameter, Eq. (5.1)
P	internal axial load on beam, Eq. (5.41)
$\bar{P}_b$	end load on beam, Fig. 4.2

$(q_{22})_i$	Eq. (5.19)
q_y, q_z	lateral loads on beam in y and z directions, Eq. (5.41)
Q_{22}	transverse shear on plate, Eq. (4.17a) and Eq. (5.12)
$Q_{11}^{\kappa}, Q_{22}^{\kappa}$, etc.	orthotropicity constants, Eq. (4.2)
$(\bar{Q}_{ij})_k$	stiffness constant for anisotropic plate, k^{th} layer
$\{R_1\}, \{R_2\}$	displacement coefficient matrices, Eqs. (5.26) and (5.44)
$R_{11}, R_{12}, \ldots R_{33}$	Eq. (5.5)
S_{11}^{k}	element (1, 1) of matrix $[Q_{ij}]^{-1}$, Eq. (4.3)
t_k	thickness of kth layer, Fig. 4.1
$[T_d], [T_f]$	transformation matrix, Eq. (5.32), Eq. (5.35)
T_x	torque on beam, Eq. 4.19
u, v, w	displacements of the neutral plane of a plate, Eq. (4.4)
ν_{12}, ν_{21}	Poisson's ratios of orthotropic plate, Eq. (4.2)
W, U, V	displacements constants of beam, Eqs. (5.40)
x, y, z	local coordinates, Fig. 4.1
$[X_1], [X_2], [X_3^{\pm}]$	matrices in Eqs. (5.25), (5.29), (5.33) and (5.34) respectively
$[X_4^{\pm}], [X_5], [X_6]$	matrices in Eqs. (5.36), (5.37), (5.44) and (5.47) respectively
$[X_7], [X_8], [X_9^{\pm}]$	matrices in Eqs. (5.50), (5.53), (5.61) respectively
$[X_{10}^{\pm}]$	matrices in Eqs. (5.62)
y_o, z_o	distances of offset in y and z directions, Fig. 5.2
z	distance to neutral plane, Eq. (4.4)
z_n	distance of neutral axis of laminated plate, Eq. (4.3)
$1, 2, 3$	coordinates in the principle directions of orthotropicity, Fig. 4.1
$[\ ]$	rectangular or square matrix
$\{\ \}$	column matrix
$\lfloor \ \rfloor$	diagonal matrix
$(\ )_{,x}$	$\partial(\ )/\partial x$
α, β	wave-mode parameter, Eqs. (5.1) and (5.18)
$\sigma_x, \sigma_y, \sigma_{xy}$	in-plane stress components, Eq. (4.1)
$\bar{\sigma} I_p$	beam property, Eq. (4.11), which is the averaged value of (stress times polar moment of inertia)

ϵ, γ	in-plane unit strains, Eq. (4.1)
θ	beam rotation about x-axis, Eq. (4.19)
Θ	displacement coefficient, Eq. (5.40)
ξ_1 to ξ_4	Eqs. (5.41)
$\epsilon_x, \epsilon_y, \gamma_{xy}$	in-plane strain components, Eq. (4.1)
Γ	warping constant, Eq. (4.10)
ψ	angle between global and local coordinates, Fig. 5.2
ω, ϕ, η, ρ	Eqs. (5.14) to (5.17)

Superscripts

k	numbering of lamina layers
+	quantities related to side of plate at $y = +b/2$
−	quantities related to side of plate at $y = -b/2$

Subscripts

BG	quantity belongs to beam element, global coordinates
BS	quantity belongs to beam element, local coordinates
G	refer to global coordinates
(1),(2),etc.	element numbers, Figs. 5.1, 5.3, 5.4
i	numbering of characteristic roots
ij	matrix element subscript
k	numbering of lamina layers
PG	quantity belongs to plate element, global coordinate
PS	quantity belongs to plate element, local coordinates
RG	restraining forces, global coordinates, Eq. (5.57)
s	refer to offset center "S"
u,v,w	along directions of x, y, and z respectively

3. INTRODUCTION

There have been numerous publications on general and local instabilities of structure components under axial compression that are made of flat plates and beam-like elements. To cite a few, Ramberg and Levy[1]* studied open section extrusions in which local instability was estimated by buckling of flanges taken as plates with suitable edge conditions and general instability analyzed by treating the extrusion as a column. Similar approximations were used in Goodman and Boyd[2] and Goodman's[3] studies of bulb-reinforced flanges. For structural sections, such as Z, T, channels and hat-type sections, and isotropic plates stiffened by such sections, a usual practice of analysis is to treat them as an assemblage of flat plate elements connected rigidly along the straight boundaries and each element has the same sinusoidal axial mode. The plate is usually taken as infinitely wide and the constraints on its sides are then neglected.

Since a thin plate is rather stiff in the in-plane directions, the common junction between two plate elements can be taken approximately as simply supported as far as lateral displacement is concerned. This simplification reduces analytical work considerably and makes possible some approximate solutions such as moment-distribution[4]. However, when this simple-support assumption is removed, one needs not only to consider the lateral displacements at the junction, but also the in-plane motions thereof induced by buckling. Thus, a rigorous theory should consider the stiffened plate as an assemblage of a single or repeated stiffened panels which consist of a series of flat thin strips, continuously connected with each other at their edges and no restraints assumed. In this category, one thinks of flat plates reinforced by structural sections and sandwiches with corrugated core. It is possible to derive, in a rigorous manner, a unified approach for a buckling analysis which need not distinguish between the so-called local modes and the general modes. The lowest load level that causes any plate element to initiate a buckling deformation before the others do (local modes) or causes several plate elements to have simultaneous deformation (general modes) is the buckling load of the stiffened plate or section. The unified approach which seems to be the most exact at the present stage of development can be represented, for example, by Wittrick's paper[5], and some analyses of similar nature but with various degrees of exactness and generality can be seen in Refs. 6 through 12.

The present analysis brings the research on stiffened plates and sections another step forward. Here the basic building blocks of the unified approach, that is, the flat plate element and the beam element that is used to represent beams, lips and beads of flanges, have been extended to unidirectional, laminated composites which, of course, include isotropic material as a particular case. The theory assumes that the orthotropic physical properties of each layer of the composites are given, i.e., E_{11}, E_{22}, G_{12}, v_{12} and v_{21} ($v_{21} = v_{12}E_{22}/E_{11}$), and the usual Kirchhoff-Love assumption regarding plane section remains plane

---

*References are collected at the end of the text

5

is valid. Lips and beads of a flange are regarded as beams elastically attached to the side of the flange, and the coupling between axial load and the curvature change is neglected. If the bead is composite reinforced, its physical properties are calculated in an approximate manner. The eccentricity of connections between plate elements and between plates and beads as well as conditions of all unloaded edges of the plate elements are considered in the analysis.

Since in most cases where fiber reinforced composites are being used as reinforcements in structural sections, the direction of the fiber always runs in the same direction as the axis of the section, the stress-strain equations used in the analysis are restricted to this type of orthotropicity. This simplification, which does not limit the generality of the present theory, reduces greatly the complexity of algebraic manipulations in the analysis as well as in the computer programs. If one needs to accommodate thermal effects and arbitrarily inclined laminated composites in the analysis, one needs only to use the appropriate stress-strain relationships in the beginning of the derivations. These equations are available in existing literature, for example, Refs. 13 and 14.

In the following text, the basic equations for laminated plates and beams were derived and the geometric and natural boundary equations necessary for enforcing continuity and equilibrium along the junctions of plate and beam elements were developed. Effects of offsets were incorporated in the equations. Elastic instability under uniaxial compression on composite reinforced plates, structural sections reinforced by composites and beaded stiffeners, and finally, stiffened plates reinforced by composites were studied. Buckled shapes from eigenvector solutions are calculated which can be used to ascertain local and general type buckling modes. The accuracy of the analysis and the associated computer programs were checked first by correlation with corresponding isotropic plates, sections and stiffened plates, then calculations were extended to sections and stiffened plates with composites. The corresponding computer programs are described in the following documents: (Refs. 15a,b,c) -- BUCLAP - Program Documents for Buckling Analysis of Laminated Composite Plates; -- BUCLAS - Program Documents for Buckling Analysis of Composite Reinforced Structural Sections; -- BUCLASP - Program Documents for Buckling Analysis of Composite Reinforced Stiffned Plates. It is expected that these computer programs will be distributed to the public through COSMIC, NASA's computer program distribution point at the University of Georgia.

The main text of the report which contains the general theory and derivations and correlations with existing analyses and tests is a complete document. Some peripheral equations and correlations of secondary importance, together with details of geometry of test specimens, are contained in the Appendix which, void of Nomenclatures and accompanying figures, should be read together with the main text for a complete understanding.

6

4. BASIC EQUATIONS

The first part of this section describes the various material and geometric constants used in the analysis. Next, the basic equations for orthotropic laminated flat plates and laminated beams, which will be used in the buckling analysis of section 5, are presented.

Plates composed of orthotropic laminas

In the following derivations, each lamina is assumed to be in a state of plane stress. For an orthotropic lamina, the stress-strain relationships are given by[14]:

$$\left\{ \begin{array}{c} \sigma_x^k \\ \sigma_y^k \\ \sigma_{xy}^k \end{array} \right\} = \left[\begin{array}{ccc} Q_{11}^k & Q_{12}^k & 0 \\ Q_{12}^k & Q_{22}^k & 0 \\ 0 & 0 & Q_{66}^k \end{array} \right] \left\{ \begin{array}{c} \epsilon_x \\ \epsilon_y \\ \gamma_{xy} \end{array} \right\} = [Q_{ij}^k] \left\{ \begin{array}{c} \epsilon_x \\ \epsilon_y \\ \epsilon_{xy} \end{array} \right\} \tag{4.1}$$

where the superscript k denotes lamina number and the elastic constants are given by

$$\begin{aligned} Q_{11}^k &= E_{11}/(1 - \nu_{21}\nu_{12}) \\ Q_{22}^k &= E_{22}/(1 - \nu_{21}\nu_{12}) \\ Q_{12}^k &= \nu_{21}E_{11}/(1 - \nu_{21}\nu_{12}) = \nu_{12}E_{22}/(1 - \nu_{21}\nu_{12}) \\ Q_{66}^k &= G_{12} \end{aligned} \tag{4.2}$$

The x, y, and z axes for the present orthotropic plate are assumed to be identical with the principle directions of the laminates 1, 2 and 3, respectively as shown in Figure 4.1. A distance z_n locates the neutral plane with respect to an arbitrary reference plane. This neutral plane is determined by calculating the resultant of the uniaxial forces in the laminas for a constant and uniform strain across the thickness.

Thus,

$$z_n = \left(\sum_{k=1}^{\ell} \frac{1}{2} \cdot \frac{1}{S_{11}^k} t_k (h_{k+1} + h_k) \right) / \left(\sum_{k=1}^{\ell} t_k \cdot \frac{1}{S_{11}^k} \right) \tag{4.3}$$

where S_{11}^k is the first element of the matrix $[Q_{ij}^k]^{-1}$, where $[Q_{ij}^k]$, being associated with kth lamina, is given in Eq. (4.1).

For an orthotropic laminated flat plate, the strain-displacement relationships are

$$
\left\{ \begin{array}{c} \varepsilon_x \\ \varepsilon_y \\ \gamma_{xy} \end{array} \right\} = \left\{ \begin{array}{c} u_{,x} \\ v_{,y} \\ u_{,y}+v_{,x} \end{array} \right\} -z \left\{ \begin{array}{c} w_{,xx} \\ w_{,yy} \\ 2w_{,xy} \end{array} \right\} \tag{4.4}
$$

where z = distance from the point to neutral plane; u, v, and w are the displacements of the neutral plane.

Substitution of Eq. (4.4) in Eq. (4.1) and integrating over the thickness of the laminas, the stress resultants N and couples M acting in the neutral plane of the plate can be expressed in terms of neutral plane displacements u, v and w as:

$$
\left\{ \begin{array}{c} N_{11} \\ N_{22} \\ N_{12} \end{array} \right\} = \left[\begin{array}{ccc} A_{11} & A_{12} & 0 \\ A_{12} & A_{22} & 0 \\ 0 & 0 & A_{66} \end{array} \right] \left\{ \begin{array}{c} u_{,x} \\ v_{,y} \\ u_{,y}+v_{,x} \end{array} \right\}
$$

$$
- \left[\begin{array}{ccc} B_{11} & B_{12} & 0 \\ B_{12} & B_{22} & 0 \\ 0 & 0 & B_{66} \end{array} \right] \left\{ \begin{array}{c} w_{,xx} \\ w_{,yy} \\ 2w_{,xy} \end{array} \right\} \tag{4.5}
$$

$$
\left\{ \begin{array}{c} M_{11} \\ M_{22} \\ M_{12} \end{array} \right\} = \left[\begin{array}{ccc} B_{11} & B_{12} & 0 \\ B_{12} & B_{22} & 0 \\ 0 & 0 & B_{66} \end{array} \right] \left\{ \begin{array}{c} u_{,x} \\ v_{,y} \\ u_{,y}+v_{,x} \end{array} \right\}
$$

$$
- \left[\begin{array}{ccc} D_{11} & D_{12} & 0 \\ D_{12} & D_{22} & 0 \\ 0 & 0 & D_{66} \end{array} \right] \left\{ \begin{array}{c} w_{,xx} \\ w_{,yy} \\ 2w_{,xy} \end{array} \right\} \tag{4.6}
$$

where the A, B, and D coefficient matrices define the overall extensional, coupling and bending stiffnesses, respectively, of the laminated orthotropic flat plate. Figure 4.1 shows also the sign conventions.

The elements of the A, B, and D matrices are given by[14]:

$$A_{ij} = \sum_{k=1}^{\ell} Q_{ij}^k \cdot t_k \qquad (4.7)$$

$$B_{ij} = \frac{1}{2} \sum_{k=1}^{\ell} Q_{ij}^k \ (h'_{k+1} + h'_k) \cdot t_k \qquad (4.8)$$

$$D_{ij} = \frac{1}{3} \sum_{k=1}^{\ell} Q_{ij}^k \ (h'^2_{k+1} + h'_{k+1} \cdot h'_k + h'^2_k) \cdot t_k \qquad (4.9)$$

where h'_k, shown in Figure 4.1, is the distance from the neutral plane to the surface of the respective lamina ($h'_k = h_k - z_n$). It is to be noted that the B matrix is responsible for the coupling between the membrane stresses and the bending of the neutral plane. For symmetrically laminated orthotropic plates in which the mid-plane is the neutral plane, matrix B vanishes and coupling does not exist.

If the orientations of the fibers of a lamina are not parallel or perpendicular to the axes of the plate, the plate is anisotropic. Then the A, B, and D matrices in Eqs. (4.5) and (4.6) will be fully populated and the quantities (Q_{ij}^k) should be replaced by their corresponding transformed quantities (designated as $(\bar{Q}_{ij})_k$ in Ref. 14) in Eqs. (4.7) to (4.9). Since the present study involves plates, structural sections and stiffened plates with uniaxial orthotropic laminas only, these anisotropic equations are not given here. They can be found, for example, in Ref. 14. The specialized stiffness matrices A, B and D (Eqs. (4.5) and (4.6)), however, can be used to approximate the behavior of anisotropic plates. For example, when skewed laminas are symmetric to the middle plane of the plate, skewed orthotropic laminas can be analyzed in the present analysis because these skewing constants, such as A_{16}, B_{16}, D_{16}, etc., appearing in Eqs. (4.5) and (4.6) would be either zero or very small compared with A_{11}, B_{11} and D_{11}, etc. and can be neglected. This approximation usually requires the existence of several alternating angle plies in the laminate.

Orthotropic laminated beams

Beads or lips in structural sections, beam-type boron reinforcements and joints with fillet, such as corners of extruded structural sections, can be idealized as beams and treated in the analysis. The origin of coordinates of its cross section is chosen, for convenience, at the geometric center of the section. The basic material properties involved are the individual lamina constants, E_{11}^k and G_{23}^k for the kth lamina.

The overall stiffnesses considered for the laminated beam-type elements are $E_{11} I_{yy}$, $E_{11} I_{zz}$, $E_{11} \Gamma$, $E_{11} A_b$, $\bar{\sigma} I_p$ and $G_{23} J$. These are estimated in an approximate manner as follows:

$$E_{11} F = \sum_{k=1}^{\ell} E_{11}^k F^k \qquad (4.10)$$

where F denotes I_{yy}, I_{zz}, Γ or A_b (I_{xx}^k and I_{yy}^k are moments of inertia about the neutral axis of the beam), and

$$\bar{\sigma}\, I_p = \sum_{k=1}^{\ell} \bar{\sigma}^k\, I_p^k \tag{4.11}$$

The above equations are based on the assumption that plane sections of the beam cross section remain plane during deformation. F^k and I_p^k for each lamina are calculated with respect to the axes chosen at the geometric center of the overall beam section. The uniform compressive stress in k^{th} lamina due to the external axial load, denoted as $\bar{\sigma}^k$, is calculated on the assumption that the axial strain is the same in all laminas.

The overall torsional stiffness of beams whose sections are made of concentric circular layers or concentric rectangular box-type layers can be expressed as

$$G_{23}\, J = \sum_{k=1}^{\ell} G_{23}^k\, J^k \tag{4.12}$$

For beams whose cross section is rectangular and is composed of layered thin plates, Eq. (4.12) would not be appropriate, since each lamina deforms with a different eccentricity towards the shear center of the overall section. In lacking an exact torsional stiffness expression for layered composite rectangular sections, the following approximate equation has been used:

$$G_{23}\, J = [(\sum_{k=1}^{\ell} G_{23}^k\, A_b^k)/(\sum_{k=1}^{\ell} A_b^k)](J_{\text{overall section}}) \tag{4.13}$$

where A_b^k is the cross sectional area of the kth layer. Physical properties of these circular and rectangular cross section beams can be found in Refs. 1, 15, 16 and 17.

Equilibrium equations and boundary conditions

The equilibrium equations for a flat plate under in-plane compressive force resultants $\bar{N}_{11}$, $\bar{N}_{22}$ and shear resultant $\bar{N}_{12}$, can be written as:

$$\frac{\partial N_{11}}{\partial x} + \frac{\partial N_{12}}{\partial y} = 0 \tag{4.14}$$

$$\frac{\partial N_{22}}{\partial y} + \frac{\partial N_{12}}{\partial x} = 0 \tag{4.15}$$

$$\frac{\partial^2 M_{11}}{\partial x^2} + \frac{\partial^2 M_{22}}{\partial y^2} + 2\frac{\partial^2 M_{12}}{\partial x \partial y} + \bar{N}_{11}\frac{\partial^2 w}{\partial x^2} + \bar{N}_{22}\frac{\partial^2 w}{\partial y^2} + 2\bar{N}_{12}\frac{\partial^2 w}{\partial x \partial y} = 0 \tag{4.16}$$

The corresponding boundary conditions, say, at ends along y-axis, are

$$w = 0 \quad \text{or} \quad Q_{22} = \frac{\partial M_{22}}{\partial y} + 2\frac{\partial M_{12}}{\partial x} + \bar{N}_{22}\frac{\partial w}{\partial y} + \bar{N}_{12}\frac{\partial w}{\partial x} = 0 \tag{4.17a}$$

10

$$\frac{\partial w}{\partial y} = 0 \quad \text{or} \quad M_{22} = 0 \tag{4.17b}$$

$$u = 0 \quad \text{or} \quad N_{12} = 0 \tag{4.17c}$$

$$v = 0 \quad \text{or} \quad N_{22} = 0 \tag{4.17d}$$

The equilibrium equations for the laminated beams are derived from elementary beam theory in which the axial load $\bar{P}_b$ due to externally applied force is acting on the neutral axis and no eccentricity is involved. Considering a beam under torsion plus axial and lateral loads, the internal forces (Fig. 4.2) at any section of the beam can be written in terms of the applied loads and displacements u,*

$$q_z = E_{11} I_{yy} (d^4 w/dx^4) + \bar{P}_b (d^2 w/dx^2) \tag{4.18}$$

$$dT_x/dx = E_{11} \Gamma (d^4\theta/dx^4) - (G_{23} J - \bar{\sigma} I_p)(d^2\theta/dx^2) \tag{4.19}$$

$$dP/dx = -E_{11} A_b (d^2 u/dx^2) \tag{4.20}$$

$$q_y = E_{11} I_{zz} (d^4 v/dx^4) + \bar{P}_b (d^2 v/dx^2) \tag{4.21}$$

where the rotation θ of the beam is, in fact, the same as the slope $w_{,y}$ at the edge of the plate.

In the present analysis, beam element will always be continuously and elastically connected to the edge of a plate to form a stiffener. Consequently, the boundary conditions applicable to beam elements are:

$$q_z = Q_{22} \quad dT_x/dx = -M_{22} \quad dP/dx = N_{12} \quad q_y = N_{22} \tag{4.22-25}$$

where the right-hand sides are given in Eqs. (4.17a), (4.5) and (4.6). The sign conventions are such that the beam is supposedly connected to the plate at y = b in Fig. 4.1.

5. BUCKLING ANALYSIS

The equations derived in section 4 will be applied in this section to the buckling analysis of (a) orthotropic, laminated, rectangular plates and (b) structural sections and stiffened plates built-up from laminated plates and beams. In the present linear theory, the prebuckling deformations and possible initial imperfections are ignored. The buckling load is defined as the smallest load at which a part of the structure (local instability) or the whole of the structure (general instability) starts to develop out-of-plane displacements (w-displacement) and a state of unstable equilibrium exists consistent with the constraints on the edges of the structure.

---

* Timoshenko, S. and Gere, J. M., Theory of Elastic Stability, 2nd Ed. 1961, McGraw-Hill, N. Y., p. 227

5.1 Orthotropic Laminated Plate Under Uniaxial Compression

The present method requires at least two opposite edges of the rectangular plate to be simply supported so that variables can be separated in the differential equations of equilibrium. A set of displacement functions, automatically satisfying the boundary conditions along these simply supported edges, are assumed. The boundary conditions on the other two edges are enforced in the buckling formulation. Substitution of the displacement functions in the equilibrium Eqs. (4.14) to (4.16) leads to the characteristic equation of the differential equations which in general is a polynomial of 8th degree. Corresponding to each given load there are eight roots from this characteristic equation. The displacements and the forces derived from them which are functions of these roots are then used to enforce the eight boundary conditions of the two remaining edges. This results in a set of eight homogeneous simultaneous equations. A buckling load corresponding to each axial wave number is obtained from these equations by determining the minimum value of the load for which the determinant of the coefficient matrix becomes zero. The buckling load is the smallest of such loads from varying the axial wave numbers. When all four edges of the plate are simply supported, the assumed displacement functions automatically satisfy all the boundary conditions, and the buckling load in this case is obtained in a closed form from the equilibrium equations.

Plates with two opposite sides simply supported and the other two sides elastically restrained:

As an example, assume that a unidirectional compressive load $\overline{N}_{11}$ is applied along the direction of x-axis, on two parallel simply supported edges of width b; the other two unloaded sides, of length a, are elastically restrained. The four sides are $x = 0$ and a, $y = -b/2$ and $+b/2$. Let k_u, k_v, k_w be the translational stiffnesses and k_θ the rotational stiffness of the elastic restraints. Superscripts + and - are used to denote the stiffnesses and displacements along the sides $y = -b/2$ and $+b/2$ respectively.

Displacement functions assumed are:

$$w = \sum_{i=1}^{8} W_i \sin \alpha \cdot e^{\beta} \qquad \alpha = m\pi x/a$$

$$v = \sum_{i=1}^{8} V_i \sin \alpha \cdot e^{\beta} \qquad \beta = p_i \pi y/b \qquad (5.1)$$

$$u = \sum_{i=1}^{8} U_i \cos \alpha \cdot e^{\beta}$$

The assumed displacements satisfy the simply supported edge conditions, $w = M_{11} = N_{11} = v = 0$, along $x = 0$ and a. The conditions at $y = -b/2$ and $+b/2$ are:

$\underline{y = -b/2}$ $\underline{y = +b/2}$

(i) $Q_{22} = -w^- k_w^-$ (i) $Q_{22} = w^+ k_w^+$

(ii) $M_{22} = w_{,y}^- k_\theta^-$ (ii) $M_{22} = -w_{,y}^+ k_\theta^+$

(iii) $N_{12} = -u^- k_u^-$ (5.2)   (iii) $N_{12} = u^+ k_u^+$ (5.3)

(iv) $N_{22} = -v^- k_v^-$ (iv) $N_{22} = v^+ k_v^+$

When a typical term of the displacement functions is substituted into the equilibrium Eqs. (4.14) to (4.16), and through the aid of Eqs. (4.5) and (4.6), one obtains:

$$\begin{bmatrix} R_{11} & R_{12} & \pi R_{13} \\ R_{21} & R_{22} & \pi R_{23} \\ R_{31} & R_{32} & \pi R_{33} \end{bmatrix} \cdot \begin{Bmatrix} U_i \\ V_i \\ W_i \end{Bmatrix} = 0 \qquad (5.4)$$

where

$$R_{11} = -A_{11}(m/a)^2 + A_{66}(p_i/b)^2$$

$$R_{12} = (A_{12} + A_{66})(m/a)(p_i/b)$$

$$R_{13} = B_{11}(m/a)^3 - (B_{12} + 2B_{66})(m/a)(p_i/b)^2$$

$$R_{21} = -R_{12}$$

$$R_{22} = A_{22}(p_i/b)^2 - A_{66}(m/a)^2 \qquad (5.5)$$

$$R_{23} = (B_{12} + 2B_{66})(m/a)^2(p_i/b) - B_{22}(p_i/b)^3$$

$$R_{31} = -R_{13}$$

$$R_{32} = R_{23}$$

$$R_{33} = -\bar{N}_{11}(m/\pi a)^2 + D_{11}(m/a)^4 - (2D_{12} + 4D_{66})(m/a)^2(p_i/b)^2 + D_{22}(p_i/b)^4$$

Expanding the determinant equation of Eq. (5.4), one obtains a polynomial:

$$K_8 p_i^8 + K_6 p_i^6 + K_4 p_i^4 + K_2 p_i^2 + K_0 = 0 \qquad (5.6)$$

The above equation thus yields eight values of p_i, which are real or complex conjugates and four roots are the negative of the other four.

From Eq. (5.4), U_i and V_i in Eq. (5.1) can be expressed in terms of W_i as:

$$U_i = \pi L_{2i} W_i$$

$$V_i = \pi L_{1i} W_i$$

$$(5.7)$$

where

$$L_{1i} = \frac{R_{23}R_{11} - R_{13}R_{21}}{R_{12}R_{21} - R_{22}R_{11}} \qquad i = 1, 2, \ldots, 8$$

$$(5.8)$$

$$L_{2i} = \frac{R_{13}R_{22} - R_{23}R_{12}}{R_{21}R_{12} - R_{22}R_{11}} \qquad i = 1, 2, \ldots, 8$$

The boundary conditions along the edges $y = \pm b/2$ can now be enforced. The displacement functions, with the eight p_i values from Eq. (5.6) are substituted into the eight boundary conditions (Eqs. (5.2) and (5.3)) with the aid of Eqs. (4.5) and (4.6). Eliminating U_i and V_i through the use of Eqs. (5.7), one obtains eight homogeneous simultaneous equations in W_i (i = 1 to 8) of the form $[D_B]\{W_i\} = 0$. These equations are satisfied if:

$$\left| D_B \right| = 0 \qquad\qquad (5.9)$$

where $\left| D_B \right|$ is the buckling determinant formed by the coefficients of W_i.

This 8x8 determinant can be written as

$$\begin{vmatrix} \exp(\pi p_i/2)[G_{1i} - k_w^+/\pi^3] & \cdots \\[6pt] \exp(\pi p_i/2)[G_{2i} + k_\theta^+(p_i/\pi b)] & \cdots \\[6pt] \exp(\pi p_i/2)[G_{3i} - k_u^+ L_{2i}/\pi] & \cdots \\[6pt] \exp(\pi p_i/2)[G_{4i} - k_v^+ L_{1i}/\pi] & \cdots \\[6pt] \exp(-\pi p_i/2)[G_{1i} + k_w^-/\pi^3] & \cdots \\[6pt] \exp(-\pi p_i/2)[G_{2i} - k_\theta^-(p_i/\pi b)] & \cdots \\[6pt] \exp(-\pi p_i/2)[G_{3i} + k_u^- L_{2i}/\pi] & \cdots \\[6pt] \exp(-\pi p_i/2)[G_{4i} + k_v^- L_{1i}/\pi] & \cdots \end{vmatrix} = 0 \qquad (5.10)$$

$$i = 1,2,3,\ldots,8$$

14

where

$$G_{1i} = -B_{12}L_{2i}(m/a)(p_i/b)+B_{22}L_{1i}(p_i/b)^2+D_{12}(m/a)^2(p_i/b)$$

$$-D_{22}(p_i/b)^3-2B_{66}[(m/a)(p_i/b)L_{2i}+(m/a)^2L_{1i}]+4D_{66}(m/a)^2(p_i/b)$$

$$G_{2i} = -B_{12}(m/a)L_{1i}+B_{22}L_{1i}(p_i/b)+D_{12}(m/a)^2-D_{22}(p_i/b)^2$$

$$(5.10a)$$

$$G_{3i} = A_{66}[L_{2i}(p_i/b)+L_{1i}(m/a)]-2B_{66}(m/a)(p_i/b)$$

$$G_{4i} = -A_{12}(m/a)L_{2i}+A_{22}L_{1i}(p_i/b)+B_{12}(m/a)^2-B_{22}(p_i/b)^2$$

Since the p_i values are functions of the external load $\bar{N}_{11}$ and the particular axial wave number, a closed form solution is not possible and the critical value of $\bar{N}_{11}$ has to be determined by an iterative method. For an assumed axial mode m and for an assumed value of $\bar{N}_{11}$, the p_i values from Eq. (5.6) are substituted into Eq. (5.10). If the value of the determinant is not zero, the load is increased in steps until Eq. (5.10) is satisfied. This load then is the buckling load for the assumed axial mode m. The calculation is repeated for various values of m and the minimum of all such values is the buckling load.

Simplifications are possible for plates with zero bending-stretching coupling, i.e. $B_{ij} = 0$ (Eq. (4.8)) and, consequently, u and v are independent of w and Eq. (5.10) is reduced to a 4x4 determinant.

The criteria of buckling can be given in terms of critical strain or critical load intensity. For composite reinforced stiffened plate, the critical load per unit length is different for differnt plate elements for uniform axial shortening, while critical strain is constant throughout the structure. The critical strain ε_x, assuming that the applied load is along x, is defined as the uniform axial strain ε_x in Eq. (4.1) at the instant of buckling such that the orthogonal stress σ_y^k in the kth lamina, and all the other laminas, is zero while the sum of the axial stress σ_x^k, through the thickness of the plate,is equal to the applied uniform line load $\bar{N}_{11}$. Thus, by inverting Eq. (4.1) and putting σ_y^k and σ_{xy}^k equal to zero, one arrives at an expression of the critical strain

$$\varepsilon_{cr} = \varepsilon_x = \bar{N}_{11}/(\sum_{k=1}^{\ell}(t^k/s_{11}^k)) \qquad (5.11)$$

If one assumes that the orthogonal stress resultant N_{22} is zero, instead of lamina stress σ_y^k in each lamina is zero, one arrives at the more familiar equation for orthotropic plate

$$\varepsilon_{cr} = \varepsilon_x = \bar{N}_{11}/(A_{11} - (A_{12}^2/A_{11})) \qquad (5.11a)$$

These two equations will produce the same critical strain criteria since prebuckling deformations are ignored in the present analysis.

Since derivations are similar, equations for buckling of composite plates with other boundary conditions are collected in the Appendix of the report for reference, and will not be presented here.

5.2 Orthotropic Laminated Structural Sections and Stiffened Plates Under Uniaxial Compression

In the present analysis, structural sections and stiffened plates of uniform cross-section are considered to be assembled from orthotropic laminated flat-plate and beam elements.

The intersecting angle between elements can be arbitrary and junctions of elements and unloaded edges can be elastically restrained, clamped, simply supported or free. However, the loaded edges of the elements have to be simply supported so that variables in the equilibrium equations can be separated. For each element, the assumed buckling displacement functions automatically satisfy the simply supported boundary conditions along the loaded edges. Consequently, all elements have the same axial mode (wave-length). These simply supported edges of a cross-section where the load is applied provide a line support for the plate elements and a point support for the beam elements.

Substitution of displacement functions such as Eq. (5.1) into the equilibrium equations for a laminated flat plate, Eqs. (4.14) to (4.16), leads to a characteristic equation for each element such as Eq. (5.6), which in general is a polynomial of 8th degree. Corresponding to an assumed uniform axial strain or an arbitrarily variable load intensity from element to element, but uniform in each element, there is a set of roots from this characteristic equation for each flat plate element. For the beam elements, the buckling displacements are simple trigonometric functions in the axial (longitudinal) coordinate. The displacements assumed are the translations (u, v, and w) and the rotation (θ) about the longitudinal axis. The enforcement of the continuity and equilibrium requirements along common element junctions results in a set of homogeneous, simultaneous equations. A buckling determinant is formed from the coefficient matrix of these equations. As usual, the buckling load of the structural section, or the stiffened plate, is the minimum load value among all modes (axial wave numbers) that make the determinant vanish.

It is to be noted that these buckling loads and their eigenvectors are determined from a linear exact buckling analysis. Except for the axial wave number, there is no need to stipulate a "mode" in its usual sense. Eigenvector plots can be used to indicate whether the buckling deformation is local or general. In contrast, the classical buckling analysis usually assumes one of the following individual buckling modes, in what is commonly known flexural (Euler) mode, torsional mode, local mode, coupling mode, etc. Such simplifying restrictions may result in missing the lowest buckling load.

Element idealization of structural sections and stiffened plates

As a typical example, consider the arbitrary structural section shown in Figure 5.1. Here Y, Z are the global axes (X-axis coincides with the axis of the section or the stiffened plate) and y, z axes are the local coordinates of each component element. Local coordinates are chosen at the geometric center of beam elements and neutral planes of plate elements. The dash-line contour in Fig. 5.1 shows the boundary of the cross section of the stiffened plate; the solid line in the interior is the neutral plane of each segment, from which offsets between neighboring elements are to be measured. The position of the neutral plane can be calculated from the mid-plane and Eq. (4.3).

Flat plate element-forces and displacements in local coordinates

Consider a typical cross section of an orthotropic laminated flat plate element as shown in Fig. 4.1. The axis y is placed at the middle of the plate. The forces and displacements along the edges $y = \pm b/2$ are initially determined with reference to the neutral plane. The forces involved are:

$$Q_{22}(= M_{22,y} + 2M_{12,x}), M_{22}, N_{12} \text{ and } N_{22} \tag{5.12}$$

The displacements involved are:

$$w, u, v \text{ and } w_{,y} \tag{5.13}$$

The overall stiffnesses A_{ij}, B_{ij} and D_{ij} are evaluated as per Eqs. (4.7) to (4.9).

Assuming that the coupling matrix B_{ij} does not vanish, the buckling displacements are stipulated as:

$$w = \sum_{i=1}^{8} e^{\beta} W_i \sin\alpha = \sum_{i=1}^{8} \omega_i W_i \sin\alpha \tag{5.14}$$

$$u = \sum_{i=1}^{8} \pi L_{2i} e^{\beta} W_i \cos\alpha = \sum_{i=1}^{8} \eta_i W_i \cos\alpha \tag{5.15}$$

$$v = \sum_{i=1}^{8} \pi L_{1i} e^{\beta} W_i \sin\alpha = \sum_{i=1}^{8} \rho_i W_i \sin\alpha \tag{5.16}$$

and then, by differentiation,

$$\theta = w_{,y} = \sum_{i=1}^{8} (\pi p_i/a) e^{\beta} W_i \sin\alpha = \sum_{i=1}^{8} \phi_i W_i \sin\alpha \tag{5.17}$$

where, in these equations,

$$\alpha = m\pi x/a \qquad\qquad \beta = \pi p_i y/a \tag{5.18}$$

17

and symbols ω_i, ϕ_i, η_i, and ρ_i are self-evident. Equilibrium equations, Eqs. (4.14) to (4.16), are satisfied when p_i are the roots of the characteristic equation, Eq. (5.6), and L_{1i}, L_{2i} are given by Eqs. (5.8). For the present axial compression case, N_{11} is the only buckling load involved.

Using the above displacements, the forces shown in Eq. (5.12) are evaluated through Eqs. (4.5) and (4.6), the results are

$$Q_{22} = \sum_{i=1}^{8} \{-B_{12}(m/a)(p_i/a)L_{2i} + B_{22}L_{1i}(p_i/a)^2$$

$$+ D_{12}(m/a)^2(p_i/a) - D_{22}(p_i/a)^3$$

$$- 2B_{66}[(m/a)(p_i/a)L_{2i} + (m/a)^2 L_{1i}]$$

$$+ 4D_{66}(m/a)^2(p_i/a)\}W_i \pi^3 e^\beta \sin\alpha$$

$$= \sum_{i=1}^{8} (q_{22})_i \, W_i \, \sin\alpha \qquad (5.19)$$

$$M_{22} = \sum_{i=1}^{8} \{-B_{12}(m/a)L_{2i} + B_{22}(p_i/a)L_{1i}$$

$$+ D_{12}(m/a)^2 - D_{22}(p_i/a)^2\}W_i \pi^2 e^\beta \sin\alpha$$

$$= \sum_{i=1}^{8} (m_{22})_i \, W_i \, \sin\alpha \qquad (5.20)$$

$$N_{12} = \sum_{i=1}^{8} \{A_{66}[(p_i/a)L_{2i} + (m/a)L_{1i}]$$

$$- 2B_{66}(p_i/a)(m/a)\}W_i \pi^2 e^\beta \cos\alpha$$

$$= \sum_{i=1}^{8} (n_{12})_i \, W_i \, \cos\alpha \qquad (5.21)$$

18

$$N_{22} = \sum_{i=1}^{8} \{-A_{12}(m/a)L_{21} + A_{22}(p_i/a)L_{11} + B_{12}(m/a)^2$$

$$- B_{22}(p_i/a)^2\} W_i \pi^2 e^\beta \sin\alpha$$

$$= \sum_{i=1}^{8} (n_{22})_i W_i \sin\alpha \qquad\qquad (5.22)$$

The quantities $(q_{22})_i$, $(m_{22})_i$, $(n_{12})_i$ and $(n_{22})_i$, similar to ω_i, ϕ_i, η_i and ρ_i in Eqs. (5.36) to (5.39), are functions of the external load $\bar{N}_{11}$ and the axial mode m.

Similar equations corresponding to a plate with u and v not coupled with w ($B_{ij} = 0$) will not be presented. These equations, together with all such equations which correspond to a particular case of the general case derived here are collected in the Appendix for reference.

Transformations to the reference plane

The above forces and displacements, which take the neutral plane as reference, have to be transferred to the line where interelement matching is done.

Let y_0 and z_0 be defined as the offsets from an element neutral plane to the line where interelement continuity is to be met. These offsets are measured along the local axes, with origin in the neutral plane, as shown in Fig. 5.2, where forces and displacements at point $B(y = +b/2)$ are to be transferred to point S. The offsets y_0 and z_0 shown here are taken as positive, since they are in the positive directions of the local axes.

In Fig. 5.2, the axes at point S are parallel to the local coordinate system y, z at point 0. The transformation of the displacements at B to S is purely a geometrical, rigid-body transfer; elasticity between these two points is neglected since the distance is small and consequently the effect would be of secondary importance. Thus, we have displacements at point S in terms of u, v and w at B:

$$w_s = w + y_0 \, w_{,y}$$
$$\theta_s = (w_{,y})_s = w_{,y}$$
$$u_s = u - z_0 \, w_{,x} + y_0 \, u_{,y} \qquad\qquad (5.23)$$
$$v_s = v - z_c \, w_{,y}$$

The subscript s indicates the new displacements at point S.

Substitution of Eqs. (5.14) to (5.17) into Eqs. (5.23) yields, for $B_{ij} \neq 0$,

$$w_s = \sum_{i=1}^{8} (\omega_i + y_o \phi_i) W_i \sin\alpha$$

$$\Theta_s = (w_{,y})_s = \sum_{i=1}^{8} \phi_i W_i \sin\alpha$$

$$\quad (5.24)$$

$$u_s = \sum_{i=1}^{8} [\eta_i - z_o(m\pi/a)\omega_i + y_o(\pi p_i/a)\eta_i] W_i \cos\alpha$$

$$v_s = \sum_{i=1}^{8} (\rho_i - z_o \phi_i) W_i \sin\alpha$$

Or written in matrix form:

$$
\begin{Bmatrix} w_s \\ \Theta_s \\ u_s \\ v_s \end{Bmatrix} = \begin{bmatrix} X_1 \\ (4 \times 8) \end{bmatrix} \begin{Bmatrix} W_1 \\ \cdot \\ \cdot \\ W_8 \end{Bmatrix}
$$

$$\quad (5.25)$$

that is,

$$\{d_{PS}\} = [X_1] \{R_1\} \quad (5.26)$$

the new notations are self-evident.

In a similar manner, the forces along the edge $y = +b/2$ when transferred to a parallel edge through S, become

$$(Q_{22})_s = Q_{22} - z_o N_{12,x}$$

$$(M_{22})_s = M_{22} + y_o Q_{22} - z_o N_{22}$$

$$\quad (5.27)$$

$$(N_{12})_s = N_{12}$$

$$(N_{22})_s = N_{22} - y_o N_{12,x}$$

20

and, from Eqs. (5.19) to (5.22), the above equations become, for $B_{ij} \neq 0$,

$$(Q_{22})_s = \sum_{i=1}^{8} [(q_{22})_i + z_o(n_{12})_i(m\pi/a)]W_i \sin\alpha$$

$$(M_{22})_s = \sum_{i=1}^{8} [(m_{22})_i + y_o(q_{22})_i - z_o(n_{22})_i]W_i \sin\alpha$$

(5.28)

$$(N_{12})_s = \sum_{i=1}^{8} (n_{12})_i W_i \cos\alpha$$

$$(N_{22})_s = \sum_{i=1}^{8} [(n_{22})_i + y_o(n_{12})_i(m\pi/a)]W_i \sin\alpha$$

which can be written in a matrix form:

$$\begin{Bmatrix} (Q_{22})_s \\ (M_{22})_s \\ (N_{12})_s \\ (N_{22})_s \end{Bmatrix} = \begin{bmatrix} X_2 \\ (4\times8) \end{bmatrix} \begin{Bmatrix} W_1 \\ \cdot \\ \cdot \\ W_8 \end{Bmatrix}$$

(5.29)

i.e.

$$\{f_{PS}\} = [X_2]\{R_1\}$$

(5.30)

$\{f_{PS}\}$ is self-evident.

Equations (5.26) and (5.30) represent the four displacements and four stress resultants, originally acting at $y = +b/2$, now transferred to the offset point S (with positive offsets y_o and z_o) in terms of the displacements at the neutral plane of the plate.

Flat plate element-forces and displacements in global coordinates

Figure 5.2 also shows the neutral plane AB of a flat plate element and its local coordinates y, z which makes a clockwise-positive angle ψ with the global coordinates X, Y, Z. The subscript G refers to the global coordinate and the subscript s indicates the local coordinate at point S.

21

Transformed to the global axes, the four displacements of Eqs. (5.25) become:

$$\begin{Bmatrix} w_G \\ \theta_G \\ u_G \\ v_G \end{Bmatrix} = \begin{bmatrix} \cos\psi & 0 & 0 & \sin\psi \\ 0 & 1 & 0 & 0 \\ 0 & 0 & 1 & 0 \\ -\sin\psi & 0 & 0 & \cos\psi \end{bmatrix} \begin{Bmatrix} w_s \\ \theta_s \\ u_s \\ v_s \end{Bmatrix} \qquad (5.31)$$

Equation (5.31) can be written simply as

$$\{d_{PG}\} = [T_d]\{d_{PS}\} \qquad (5.32)$$

In the following text, superscripts $+$ and $-$ will be used with various matrix designations (for example, d_{PG}^+, d_{PG}^-, X_3^+, etc.) to differentiate the corresponding quantities at sides $y = +b/2$ and $y = -b/2$ respectively, for the flat plate element. Thus, when y in β of Eq. (5.18) is made to be equal to $+b/2$, we shall use $[X_1^+]$ in Eq. (5.26) and when $y = -b/2$, $[X_1]$ becomes $[X_1^-]$. Consequently, substitution of Eq. (5.26) into Eq. (5.32) yields, for $B_{ij} \neq 0$,

$$\{d_{PG}^+\} = [T_d][X_1^+]\{R_1\} = [X_3^+]\{R_1\} \qquad y = +b/2 \qquad (5.33)$$

$$\{d_{PG}^-\} = [T_d][X_1^-]\{R_1\} = [X_3^-]\{R_1\} \qquad y = -b/2 \qquad (5.34)$$

Similar to the transformations of displacements, local coordinate forces of Eqs. (5.29) are transformed to the global coordinates by:

$$\begin{Bmatrix} (Q_{22})_G \\ (M_{22})_G \\ (N_{12})_G \\ (N_{22})_G \end{Bmatrix} = \begin{bmatrix} \cos\psi & 0 & 0 & \sin\psi \\ 0 & -1 & 0 & 0 \\ 0 & 0 & 1 & 0 \\ 0 & -\sin\psi & 0 & \cos\psi \end{bmatrix} \begin{Bmatrix} (Q_{22})_s \\ (M_{22})_s \\ (N_{12})_s \\ (N_{22})_s \end{Bmatrix} \qquad (5.35)$$

Let $[T_f]$ represent the square transform matrix in Eq. (5.35). Substitution of Eq. (5.30) into the right-hand side of Eq. (5.35) and by putting $y = +b/2$ and $-b/2$ respectively, one obtains the following equations to represent the plate forces in global coordinate:

$$\{f_{PG}^+\} = [T_f][X_2^+]\{R_1\} = [X_4^+]\{R_1\} \qquad y = +b/2 \qquad (5.36)$$

$$\{f_{PG}^-\} = [T_f][X_2^-]\{R_1\} = [X_4^-]\{R_1\} \qquad y = -b/2 \qquad (5.37)$$

Equations (5.33), (5.34), (5.36), and (5.37) are displacements and forces in global coordinate at the edges $y = +b/2$ and $-b/2$ of a flat plate element in terms of the eight amplitude constants W_1 to W_8 for that element.

Beam element - forces and displacements in local coordinates

The beam elements are idealized as a line through their geometric center in the longitudinal direction. The forces and displacements involved in interelement equilibrium and continuity are at first determined along this line and then transformed. The forces involved are:

$$q_z \ , \quad dT_x/dx \ , \quad dP/dx \ , \quad \text{and} \quad q_y \tag{5.38}$$

The displacements involved are:

$$w \ , \quad \theta \ , \quad u \quad \text{and} \quad v \tag{5.39}$$

The positive directions of the displacements and forces with respect to the local coordinate are shown in Fig. 5.2.

The buckling displacements are assumed as

$$w = W \sin\alpha \qquad \theta = \Theta \sin\alpha \qquad v = V \sin\alpha \qquad u = U \cos\alpha \tag{5.40}$$

where α is equal to $m\pi x/a$ as given in Eq. (5.18). These displacements satisfy the simply supported conditions at $x = 0$ and $x = a$ where the external compressive force is applied.

Substitution of Eqs. (5.40) into Eqs. (4.18) to (4.21) yields

$$q_z = [E_{11}I_{yy}(m\pi/a)^4 - \bar{P}_b(m\pi/a)^2]W \sin\alpha = W \xi_1 \sin\alpha$$

$$dT_x/dx = [E_{11}\Gamma(m\pi/a)^4 + G_{12}J(m\pi/a)^2 - \bar{\sigma}I_p(m\pi/a)^2]\Theta \sin\alpha = \Theta \xi_2 \sin\alpha$$

$$dP/dx = [E_{11}A_b(m\pi/a)^2]U \cos\alpha = U \xi_3 \cos\alpha$$

$$q_y = [E_{11}I_{zz}(m\pi/a)^4 - \bar{P}_b(m\pi/a)^2]V \sin\alpha = V \xi_4 \sin\alpha \tag{5.41}$$

Similar to the flat plate elements, the transformation of force and displacement at the geometric axis of the beam to the offset axis can be done purely on geometric considerations. Figure 5.2 can also be used to show the offset axis S and the geometric axis 0 of the beam with point 0 being moved to point B.

23

The displacements of Eq. (5.39) when transferred to the offset axes become:

$$w_s = w + y_o \theta$$
$$\theta_s = \theta$$
$$u_s = u - z_o w_{,x} - y_o v_{,x}$$
$$v_s = v - z_o \theta$$

(5.42)

where the subscript s refers to the offset axis at S. After substitution from Eq. (5.40), the above equations become:

$$
\begin{Bmatrix} w_s \\ \theta_s \\ u_s \\ v_s \end{Bmatrix} =
\begin{bmatrix}
0 & 0 & \sin\alpha & y_o \sin\alpha \\
0 & 0 & 0 & \sin\alpha \\
\cos\alpha & -y_o(m\pi/a)\cos\alpha & -z_o(m\pi/a)\cos\alpha & 0 \\
0 & \sin\alpha & 0 & -z_o \sin\alpha
\end{bmatrix}
\begin{Bmatrix} U \\ V \\ W \\ \Theta \end{Bmatrix}
$$

(5.43)

or, written symbolically,

$$\{d_{BR}\} = [X_5]\{R_2\}$$

(5.44)

where $[X_5]$ is a 4x4 matrix. Similarly, the forces can be transformed to the offset axes as

$$(q_z)_s = q_z + (d^2 P/dx^2) z_o$$
$$(dT_x/dx)_s = dT_x/dx + q_y z_o - q_z y_c$$
$$(dP/dx)_s = dP/dx$$
$$(q_y)_s = q_y + (d^2 P/dx^2) y_o$$

(5.45)

The above equations, on substitution from Eqs. (5.41), become:

$$
\begin{Bmatrix} (q_z)_s \\ (dT_x/dx)_s \\ (dP/dx)_s \\ (q_y)_\varepsilon \end{Bmatrix} =
\begin{bmatrix}
-z_o \xi_3 (m\pi/a)\sin\alpha & 0 & \xi_1 \sin\alpha & 0 \\
0 & z_o \xi_4 \sin\alpha & -y_o \xi_1 \sin\alpha & \xi_2 \sin\alpha \\
\xi_3 \cos\alpha & 0 & 0 & 0 \\
-y_o \xi_3 (m\pi/a)\sin\alpha & \xi_4 \sin\alpha & 0 & 0
\end{bmatrix}
\begin{Bmatrix} U \\ V \\ W \\ \Theta \end{Bmatrix}
$$

or, written symbolically, as

(5.46)

24

$$\{f_{BS}\} = [X_6] \{R_2\} \tag{5.47}$$

where $[X_6]$ is a 4x4 matrix and its elements are functions of the external load $\bar{F}_b$ on the beam element. The displacements and forces of a beam element with respect to the offset line are thus given by Eqs. (5.43) and (5.46) respectively. The positive directions of these are the same as those indicated in Figure 4.2.

Beam element - forces and displacements in global coordinates

Figure 5.2 can also be used to show the global coordinates X, Y, and Z in relation to the local axes y and z of the beam where the local axis of y makes an angle ψ with the global Y axis.

Using subscript G to indicate the quantities with respect to the global axes, the four displacements of Eqs. (5.43), after transformation, become

$$\left\{\begin{array}{c} w_G \\ \theta_G \\ u_G \\ v_G \end{array}\right\} = \left[T_d \right] \left\{\begin{array}{c} w_s \\ \theta_s \\ u_s \\ v_s \end{array}\right\} \tag{5.48}$$

or

$$\{d_{BG}\} = [T_d] \{d_{BS}\} \tag{5.49}$$

where the transformation matrix $[T_d]$ is the same as in Eq. (5.32). Substituting for $\{d_{BS}\}$ from EQ. (5.44), the above equation can be written as:

$$\{d_{BG}\} = [T_d] [X_5] \{R_2\} = [X_7] \{R_2\} \tag{5.50}$$

where $[X_7]$ is a 4x4 matrix.

Using the continuity conditions of Eqs. (4.22) to (4.25), the global forces acting on the beam from the plate side, whose positive sign convention is shown in Fig. 5.2, can be expressed by

$$\left\{\begin{array}{c} (Q_{22})_G \\ (M_{22})_G \\ (N_{12})_G \\ (N_{22})_G \end{array}\right\} = \left[T_f \right] \left\{\begin{array}{c} (q_z)_s \\ (dT_x/dx)_s \\ (dP/dx)_s \\ (q_y)_s \end{array}\right\} \tag{5.51}$$

or

$$\{f_{BG}\} = [T_f] \{f_{BS}\} \tag{5.52}$$

where the transformation matrix $[T_f]$ is the same as that in Eq. (5.35).

25

Substituting for $\{f_{BS}\}$ from Eq. (5.47), the above equation becomes

$$\{f_{BG}\} = [T_f] [X_6] \{R_2\} = [X_8] \{R_2\} \qquad (5.53)$$

where $[X_8]$ is a 4x4 matrix.

Thus, $\{d_{BG}\}$ and $\{f_{BG}\}$ as given by Eqs. (5.50) and (5.53) respectively, give the displacements and forces of the beam element at offset S with respect to the global system.

5.3 Equations for Inter-element Displacement Continuity and Force Equilibrium

Figure 5.3 shows a typical joint where three plate elements join together with a beam element. The global coordinates and local coordinates of each element are shown in the figure where dash line illustrates the outline of the section. For the beam element, B is its geometric center; for the plate elements, mid-plane can be taken initially as the reference plane for convenience in measurements, however, position of neutral plane (shown in Fig. 5.3 as y-axis) should be calculated since offsets and inter-element matching of continuity are being done based on neutral axes.

Angle ψ is positive when measured clockwise from Y-axis to y-axis of the individual element. For the purpose of illustration, let B be chosen as the offset axis on which inter-element matching will be done. Consequently, the beam element with center at B has no offset.

The forces and displacements of the flat plate elements, after transformed to the offset point and converted to the global coordinates, and those of the beam elements which are already in global coordinates, are shown in Table 5.1.

Table 5.1

Forces and Displacements in Inter-Element Matching
at the Junction in Fig. 5.3

Element No.	Force and Displacement Expression	Equation No.
(1) and (4)	$\{f_{PG}^-\}$	5.37
	$\{d_{PG}^-\}$	5.34
(3)	$\{f_{PG}^+\}$	5.36
	$\{d_{PG}^+\}$	5.33
(2)	$\{f_{BG}\}$	5.53
	$\{d_{BG}\}$	5.50

As far as external loads are concerned, a junction of elements will belong to one of the following cases:

   (a) free from external loads
   (b) elastically restrained
   (c) clamped
   (d) simply supported

Detail calculations of the first two cases will be given as examples.

(a) Free junction of elements

Consider the joint shown in Fig. 5.3, since there are no external constraints, force equilibrium at B yields

$$\{f_{PG}^-\}_{(1)} + \{f_{BG}^+\}_{(2)} + \{f_{PG}^+\}_{(3)} + \{f_{PG}^-\}_{(4)} = 0 \tag{5.54}$$

and inter-element displacement continuity requirements yield

$$\{d_{PG}^-\}_{(1)} = \{d_{BG}^+\}_{(2)} = \{d_{PG}^+\}_{(3)} = \{d_{PG}^-\}_{(4)} \tag{5.55}$$

where the subscripts 1, 2, 3 and 4 with parenthesis indicate the element number. These four equations, Eqs. (5.54) and (5.55), after using the appropriate equations as shown in Table 5.1, can be written in a matrix form:

$$
\begin{bmatrix}
[X_4^-]_{(1)} & [X_8^-]_{(2)} & [X_4^+]_{(3)} & [X_4^-]_{(4)} \\
[X_3^-]_{(1)} & -[X_7^-]_{(2)} & & \\
& [X_7^-]_{(2)} & -[X_3^+]_{(3)} & \\
& & [X_3^+]_{(3)} & -[X_3^-]_{(4)}
\end{bmatrix}
\begin{Bmatrix}
\{R_1\}_{(1)} \\
\{R_2\}_{(2)} \\
\{R_1\}_{(3)} \\
\{R_1\}_{(4)}
\end{Bmatrix} = 0
$$

$$\tag{5.56}$$

where the rectangular matrix is of the size 16x28.

(b) Elastically restrained junction of elements

Let k_{UG}, k_{VG}, k_{WG} and $k_{\Theta G}$ be the four spring constants of the restraints in the direction X, Y, Z and Θ_G (Fig. 5.3) along the inter-element junction line. The appropriate restraints can be found as

$$\{f_{RG}\} = \lceil k_{RG} \rfloor \{d_{PG}^-\}_{(1)} \tag{5.57}$$

where $\{f_{RG}\}$ is the vector of restraint forces $(Q_{22})_{RG}$, $(M_{22})_{RG}$, $(N_{12})_{RG}$ and $(N_{22})_{RG}$; $\lceil k_{RG} \rfloor$ is the diagonal matrix whose diagonal elements are the spring constants k_{WG}, $k_{\Theta G}$, k_{UG} and k_{VG}; and $\{d_{PG}^-\}_{(1)}$ are the displacements

at the end of plate No. (1) transformed to the offset point B in global coordinates. The choice of the No. (1) plate is arbitrary since, through Eqs. (5.55), all elements have the same displacements at that point.

Substitution of Eq. (5.34) into Eq. (5.57) yields

$$\{f_{RG}\} = \lceil k_{RG\rfloor} [X_3^-]_{(1)} \{R_1\}_{(1)} \tag{5.58}$$

which is the external force to be added to the equilibrium equation of the joint as given in Eq. (5.54). The continuity equation is the same as Eqs. (5.55). Consequently, one needs only to replace the matrix element $[X_4^-]_{(1)}$ by $[X_4^-]_{(1)} + \lceil k_{RG\rfloor} [X_3^-]_{(1)}$ in Eq. (5.56) for the elastically restrained joint.

Boundary conditions along any unloaded flat plate element

The unloaded flat plate element can be free, elastically restrained, clamped or simply supported. The constraints and the displacements will be referred to the neutral plane of the plate.

By putting $\psi = y_o = z_o = 0$ in appropriate equations, displacements and forces at either end of a plate element can be obtained in global coordinates.

(a) Free edge

Since forces at a free edge should vanish, one obtains $\{f_{PG}^+\} = 0$, or $\{f_{PG}^-\} = 0$. From Eqs. (5.36) and (5.37), we have

$$[X_4^+] \cdot \{R_1\} = 0 \qquad\qquad \text{or} \qquad\qquad [X_4^-] \cdot \{R_1\} = 0 \tag{5.59}$$

$$\left. \rule{0pt}{2.5em}\right| \psi = y_o = z_o = 0 \qquad\qquad \left. \rule{0pt}{2.5em}\right| \psi = y_o = z_o = 0$$
$$\left. \rule{0pt}{1em}\right| y = +b/2 \qquad\qquad\qquad \left. \rule{0pt}{1em}\right| y = -b/2$$

(b) Elastically restrained edge

Similar to Eq. (5.58), let $\lceil k_{RG\rfloor}$ be the diagonal matrix whose elements are the spring constants along in neutral axis in global coordinates, then the edge conditions are

$$\left([X_4^+] + \lceil k_{RG\rfloor} [X_3^+]\right) \cdot \{R_1\} = 0$$
$$\left.\rule{0pt}{2.5em}\right| \psi = y_o = z_o = 0$$
$$\left.\rule{0pt}{1em}\right| y = +b/2$$

or

$$\left([X_4^-] + \lceil k_{RG\rfloor} [X_3^-]\right) \cdot \{R_1\} = 0 \tag{5.60}$$
$$\left.\rule{0pt}{2.5em}\right| \psi = y_o = z_o = 0$$
$$\left.\rule{0pt}{1em}\right| y = -b/2$$

(c) Clamped edge

The boundary conditions for a clamped edge are $w = w_{,y} = 0$ and two equations concerning in-plane displacements or forces, i.e., u or $N_{12} = 0$ and v or $N_{22} = 0$. If $u = 0$ and $v = 0$ are chosen, for example, the clamped edge conditions will have the same expression as Eq. (5.59) except that X_4 is replaced by X_3. If $u = 0$ and $N_{22} = 0$ are chosen, Eqs. (5.14), (5.15), (5.16) and (5.22) should be used which will lead to a 4x8 matrix designated by a new notation, say

$$[X_9^+] \cdot \{R_1\} = 0 \Big|_{y = +b/2} \quad \text{or} \quad [X_9^-] \cdot \{R_1\} = 0 \Big|_{y = -b/2} \quad (5.61)$$

(d) Simply supported edge

The classical simple support conditions are $w = M_{22} = u = N_{22} = 0$. If these four conditions are chosen, Eqs. (5.14), (5.20), (5.15) and (5.22) will lead to a 4x8 matrix, designated by

$$[X_{10}^+] \cdot \{R_1\} = 0 \Big|_{y = +b/2} \quad \text{or} \quad [X_{10}^-] \cdot \{R_1\} = 0 \Big|_{y = -b/2} \quad (5.62)$$

For convenience of reference, equations for inter-element matching and end conditions are collected in Table 5.2.

Table 5.2
Collection of Flat Plate and Beam Element Equations for
Inter-Element Matching and End Conditions ($B_{ij} \neq 0$)

Force or Displacement	Equation	Equation No.	Size of Matrix [X]	Remark
$\{d_{PG}^{\pm}\} = [X_3^{\pm}]\{R_1\}$		5.33,5.34	4x8	plate displacement
$\{f_{PG}^{\pm}\} = [X_4^{\pm}]\{R_1\}$		5.36,5.37	4x8	plate force
$\{d_{BG}\} = [X_7]\{R_2\}$		5.50	4x4	beam displacement
$\{f_{BG}\} = [X_8]\{R_2\}$		5.53	4x4	beam force
$[X_4^{\pm}]\{R_1\} = 0$		5.59	4x8	free end
$([X_4^{\pm}]+\lceil k_{RG_j} \rceil[X_3^{\pm}])\{R_1\}=0$		5.60	4x8	elastically restrained end
$[X_3^{\pm}]\{R_1\}=0$ or $[X_9^{\pm}]\{R_1\}=0$		5.61	4x8	clamped end
$[X_{10}^{\pm}]\{R_1\}= 0$		5.62	4x8	simply supported end

29

5.4 Equations for Buckling of Structural Sections and Stiffened Plates

The buckling equation for the previous structural section under uniaxial compressive load will be obtained by matching the neighboring elements together. Assuming that the left end of the section shown in Fig. 5.1 is simply supported while the right end is clamped as defined in Eq. (5.61).

Based on equations in Table 5.2 and Fig. 5.1, one obtains the following equations which enforce continuities between elements and satisfy the boundary conditions at the ends:

$$
\begin{array}{cccccccc}
(1) & (2) & (4) & (3) & (5) & (6) & (7) & (8)
\end{array}
$$

$$
\begin{bmatrix}
x_{10}^- & & & & & & & \\
x_3^+ & -x_3^- & & & & & & \\
x_4^+ & x_4^- & & & & & & \\
 & x_3^+ & -x_7 & & & & & \\
 & & x_7 & -x_3^- & & & & \\
 & x_4^+ & x_8 & x_4^- & & & & \\
 & & & x_3^+ & -x_3^- & & & \\
 & & & x_4^+ & x_4^- & & & \\
 & & & & x_3^+ & -x_3^- & & \\
 & & & & x_3^- & -x_3^- & & \\
 & & & & x_4^+ & x_4^- & x_4^- & \\
 & & & & & x_3^+ & -x_7 & \\
 & & & & & x_4^+ & x_8 & \\
 & & & & & & x_9^+ &
\end{bmatrix}
\begin{Bmatrix}
R_{1(1)} \\
R_{1(2)} \\
R_{2(4)} \\
R_{1(3)} \\
R_{1(5)} \\
R_{1(6)} \\
R_{1(7)} \\
R_{2(8)}
\end{Bmatrix} = 0
\qquad (5.63)
$$

where the numbers in parenthesis are the numbering of elements to which the appropriate quantities belong. The square matrix in Eq. (5.63) is the buckling determinant, of order 56x56. A common factor of $\sin\alpha$ and $\cos\alpha$ ($\alpha = m\pi x/a$) should be taken out from the rows of the determinant.

A second example considered is that of a hat-section stiffened plate shown in Fig. 5.4 where the stiffener dimensions and their spacing is repetitive. The stiffened plate is idealized in Fig. 5.4 into line elements

with the element numbers shown in parenthesis. The inter-element continuity and equilibrium equations, together with end equations for the end elements (1) and (29), can be written in a manner identical to Eq. (5.63). Because of repetitive nature of the stiffeners, these equations can be considered to consist of three basic parts; namely:

(i) a set of equations, say designated as $[T_a]$ $\{R_a\}$, representing the left end side of the stiffened plate,

(ii) a second set of equations, $[T_b]$ $\{R_b\}$ representing the repetitive unit. The number of repetitions of this set of equations is the same as the number of the repetitive units in the structure,

(iii) a third set of equations, $[T_c]$ $\{R_c\}$, representing the right end side of the stiffened plate.

In Fig. 5.4, the two ends and the inter-element joints are marked with a dot. The left side block consists of six dots and involves elements from (1) to (7). The first repetitive unit, as well as all the other repetitive units, contains six dots and the continuity equations involve elements from (7) to (14). Assuming that there are three such repetitive units in the plate, the right side block contains two dots and involves elements (28) and (29).

These three matrices can be written as in the following:

$$
[T_a]\{R_a\} =
\begin{array}{cccccccc}
(1) & (2) & (3) & (4) & (5) & (6) & (7) \\
\end{array}
$$

$$
[T_a]\{R_a\} =
\left[
\begin{array}{ccccccc}
X_{10}^- & & & & & & \\
X_3^+ & -X_3^- & & & & & \\
X_4^+ & X_4^- & & & & & \\
& X_3^+ & -X_3^- & & & & \\
& & X_3^- & -X_3^- & & & \\
& X_4^+ & X_4^- & X_4^- & & & \\
& & X_3^+ & & -X_3^- & & \\
& & X_4^+ & & X_4^- & & \\
& X_3^+ & & & -X_3^- & & \\
& & & & X_3^- & -X_3^- & \\
& X_4^+ & & & X_4^- & X_4^- & \\
& & X_3^+ & -X_3^+ & & & \\
& & X_4^+ & X_4^+ & & & \\
\end{array}
\right]
\left\{
\begin{array}{c}
R_{1(1)} \\ \\
R_{1(2)} \\ \\
R_{1(3)} \\ \\
R_{1(4)} \\ \\
R_{1(5)} \\ \\
R_{1(6)} \\ \\
R_{1(7)}
\end{array}
\right\}
\qquad (5.64)
$$

31

$$[T_b]\{R_b\} = \begin{matrix} (7) & (8) & (9) & (10) & (11) & (12) & (13) & (14) \end{matrix}$$

$$[T_b]\{R_b\} =
\begin{bmatrix}
x_3^+ & -x_3^- & & & & & & \\
x_4^+ & x_4^- & & & & & & \\
 & x_3^+ & -x_3^- & & & & & \\
 & x_4^+ & x_4^- & & & & & \\
 & & x_3^+ & -x_3^- & & & & \\
 & & x_3^- & -x_3^- & & & & \\
 & & x_4^+ & x_4^- & x_4^- & & & \\
 & & & x_3^+ & -x_3^- & & & \\
 & & & x_4^+ & x_4^- & & & \\
 & & & & x_3^+ & -x_3^- & & \\
 & & & & x_3^- & -x_3^- & & \\
 & & & & x_4^+ & x_4^- & x_4^- & \\
 & & & & & x_3^+ & -x_3^+ & \\
 & & & & & x_4^+ & x_4^+ &
\end{bmatrix}
\begin{Bmatrix}
R_{1(7)} \\
R_{1(8)} \\
R_{1(9)} \\
R_{1(10)} \\
R_{1(11)} \\
R_{1(12)} \\
R_{1(13)} \\
R_{1(14)}
\end{Bmatrix}$$

$$(5.65)$$

$$[T_c]\{R_c\} =
\begin{bmatrix}
x_3^+ & -x_3^- \\
x_4^+ & x_4^- \\
 & x_{10}^+
\end{bmatrix}
\begin{Bmatrix}
R_{1(28)} \\
R_{1(29)}
\end{Bmatrix}
\qquad (5.66)$$

The buckling determinant can be obtained from sub-matrices $[T_a]$, $[T_b]$ and $[T_c]$, and the eigenvectors are the column matrices $\{R_a\}$, $\{R_b\}$ and $\{R_c\}$. As in Eq. (5.63), a common factor in each row for $\sin\alpha$ or $\cos\alpha$ can be taken out in the determinantal equation and the buckling load and the corresponding eigenvectors are functions of the axial half-wave number m. The plot of the deflected shape by means of the eigenvectors are useful for determining whether buckling involves, on a relative magnitude, only local elements (local instability) or all elements (general instability). Computer sub-routines for finding eigenvectors are commonly available and such procedure will not be described here.

The structure shown in Fig. 5.4 used for the second example is a typical stiffened plate which has a number of repeated substructures. The choice

of how many elements go to the beginning eigenvector $\{R_a\}$ and how many go to the ending eigenvector $\{R_c\}$ is arbitrary. However, in the subroutine (named BLKDET) used in the program BUCLASP (Ref. 15c), a working space is provided to first store $[T_a]$ and decompose it and then repeatedly bring in $[T_b]$ for operation and finally $[T_c]$. Consequently, core storage can be saved by making $[T_c]$ as small as possible. That is the reason why $[T_c]$ is smaller than $[T_a]$ in the second example. Some techniques in handling large matrices and the convention for angles relating the orientation of one plate element to another are described in program documents, Ref. 15a, b, c, which will be distributed by NASA.

The present method has been used to correlate with other existing analyses and tests for composite plates, structural sections and stiffened plates in the next sections. As has been mentioned before, the usual practice of estimating the elastic instability of thin-walled structures is to guess possible modes based on which simplified analysis can be made. Junctions of internal members are usually taken as nodal lines about which force and moment equilibrium are satisfied to some extent but their translations are ignored. The assumption regarding possible modes requires expertise in the analysis and may miss a lower-load mode and the immovable nodal line assumption requires non-existing external forces to hold the joints which will make the structure stiffer than it is. However, when the mode is correctly assumed, the usual method may yield good agreement with more exact analysis such as the present one, as can be seen from the next sections.

6. CORRELATIONS WITH OTHER ANALYTICAL RESULTS

In correlation studies with other analytical results, the mathematical models used in others' analyses will be followed, i.e., whether a stiffener is treated as a beam or a plate in the present analysis will be consistent with those in the references.

A. Buckling of simply supported web with isotropic or orthotropic flange (Ref. 18)

In Ref. 18, the buckling of a supported web section, one side of its cross section simply supported and the other parallel side free, with and without unidirectional composite reinforcement on its flange, is studied. Two types of failure modes were examined in Ref. 18, one is a local mode and the other is a long-wave mode.

The orthotropic constants used[18] are

$$E_x = E \text{ in the direction of filament} = 30.25 \times 10^6 \text{ psi}$$

$$E_y = 2.03 \times 10^6 \text{ psi}$$

$$\nu_{xy} = 0.346 \qquad\qquad (6.1)$$

$$G_{xy} = 0.5249 \times 10^6 \text{ psi}$$

unless otherwise specified, these constants will be used in the rest of correlations where orthotropic materials are used.

33

Local mode

When the dimension of the section is such that the axial wave length is of the order of magnitude of the width of the web, one observes the so-called local mode and the results are given in Fig. 6.1 where the flange is treated as a plate. It can be seen from the curves that when the section is reinforced on the outstanding flange by composites, the flange seems stiff enough to force a node-line at the junction of the two legs. As a consequence, the approximate analysis in Ref. 18 which implies such an assumption agrees very well with the present method. On the other hand, when the flange is not reinforced, the junction seems flexible and may be displaced and the approximate analysis yields higher values than the present method.

Long-wave mode

For the long-wave mode, the same type of composite reinforced flange-web is studied where, in Ref. 18 as well as in the present method, the flange is treated as a beam. The geometry of the 15-inch long column is given in the following,

$$b_w = 1.5 \text{ in.} \qquad b_f = 0.6 \text{ in.} \qquad t_w = .05 \text{ in.} \qquad t_f = 3\, t_w$$

For the given dimensions, one half-wave yields the lowest buckling load. The present method gives a buckling parameter[18] $k_w = 1.58$ while the value in Ref. 18 is 1.56. The difference is 1%.

B. Buckling of discretely stiffened isotropic plate with a single orthotropic stiffener (Ref. 18)

Shallow orthotropic eccentric stiffener

Figure 6.2 shows the cross section of a discretely stiffened plate with an orthotropic eccentric stiffener. The stiffener is so shallow that in Ref. 18 it is treated as a beam with $G_{yz} = 0$. The boundary conditions along the unloaded sides of the plate are $w = M_{22} = N_{12} = N_{22} = 0$. In Ref. 18, displacements at the junction between the stiffener and the two parts of the plate were matched for out-of-plane displacement only. The results in Fig. 6.2 showed excellent agreement in spite of the difference in the rigor of the two analytical approaches.

Deep orthotropic eccentric stiffener

When the stiffener is deep, it is taken as an orthotropic plate in Ref. 18 where forces, moments and rotations are matched at the common boundary of the three plate elements whose lateral displacements at that joint are ignored. In Fig. 6.3, two points, marked as 1 and 2, are obtained by the present method while the solid curve is from the reference. The results agree very well.

34

C. Buckling of plates with multiple isotropic stiffeners and sandwich panels (Refs. 19, 20, 21, 22)

Figure 6.4 shows seven types of multiply stiffened plates and sandwich panels that are used to correlate with the present method. The results of correlations are given in Table 6.1 and brief descriptions are given below according to its order in the table. The exactness of the analysis in these references varied, but, in general, the translations in the joints are neglected while moment equilibriums are being maintained.

Panel 1 is an integrally stiffened plate. When the length of the plate is so proportioned to its width that the critical mode has several axial waves and the buckling load is not affected by the number of stiffeners which, for the present geometry, is about four or five stiffeners. Such a mode is called local mode in the reference[19] and the stiffeners are treated as discrete plates. The result shown in the table is based on an infinitely wide plate in the reference and for a six-stiffener plate in the present method. When the panel is long, such as a 25-inch long, six-stiffener plate, the present method shows a single half-wave mode and the buckling load is 22300 lbs. where stiffeners are treated as discrete beams. It differs by 5% with the result from Eq. (A3) of Ref. 20 which treats the stiffeners as beams with their elastic properties smeared onto the spacings.

Panels 2 and 3 are two plates with Tee and L-section stiffeners respectively. They are from the same reference as Panel 1 (Ref. 19) and used the same method. Tee and L sections are treated as discrete plate elements joined togehter with translations ignored. In the reference, the panel is taken as infinitely wide while the value given in the present method is for a six-stiffener plate.

Panel 4 is an isotropic truss-core sandwich panel. In Ref. 21, such a panel is treated by assuming various buckling modes and matching moment equilibrium in joints whose translations are ignored. The lowest load obtained by different modes is taken as the buckling load. This approach, when correctly applied, yields very good agreement with the present more exact method as can be seen in Table 6.1 where two cases are studied. The only difference in the two cases is the thickness of the wall of the core (see Fig. 6.4). Case A is for a core with equal thickness of core web and the face sheet, known as a sandwich where core restrains face because with that thickness proportion, the face sheet relies on core webs for instability support. On the other hand, case B, where the core web is only one-half as thick as the face sheet, the opposite is true. Figure 6.5 shows the mode shapes of the two cases by calculating the eigenvectors of the buckling analysis. It clearly shows that, in case A, where core-restrains-face, the face sheets near the two free edges of the panel buckled while in case B, the face sheets are thick enough to sustain the load at the free edges of the panel and it is the core web near the center of the panel that buckled first.

35

Panels 5, 6 and 7 are a corrugated sandwich panel, Zee and hat-section stiffened plates respectively, taken from Ref. 22. The method used is the same as in Ref. 19 where the stiffeners and the web of the corrugation are treated as discrete plates joined together and displacement of the joint is neglected. The values given in the reference are for infinitely wide panels while those of the present method are for finite panels. The higher buckling loads predicted by the present method are due to the fact that the flanges of the Zee and hat-section stiffeners are considered as a part of the plate in the present method while in the references the bending stiffness of the plate and the flange are calculated separately and then added together. The idealization for the stiffeners at the joints as treated in Ref. 22 is closer to a riveted attachment while that of the present method is similar to a bonded connection. It is interesting to note that tests conducted in Ref. 23 showed that the buckling stress of a bonded Zee-section stiffened plate is 19% higher than a corresponding riveted Z-stiffener plate. Incidently, this value is quite close to the 18% as indicated by Panel 6 of Table 6.1.

Table 6.1 Correlations of Analytical Results in Literature and the Present Method for the Seven Panels Shown in Fig. 6.4

| Panel | Remark | Comparison of Buckling Load | | |
		Existing * Reference	Present Method	Ratio
1	Ref. 19, stiffener as discrete plate	k_s = 1.87	1.86(m=6)	1.01
	Ref. 20, stiffener as smeared beam	P_{cr} = 23,450(1)	22,432(1)	1.04
2	Ref. 19, local mode, stiffener as plate	k_s = 4.30	4.25(5)	1.01
3	Ref. 19, Case A,	σ_{cr} = 21,400	21,300(9)	1.01
	Case B,	σ_{cr} = 42,000	41,600(6)	1.01
	Case C,	σ_{cr} = 41,100	41,900(7)	1.00
4	Ref. 21, Case A, core-restrains-face type	σ_{cr} = 16,920	16,954(7)	1.00
	Ref. 21, Case B, face-restrains-core type	σ_{cr} = 6,070	6,019(9)	1.01
5	Ref. 22	σ_{cr} = 20,400(5)	19,550(5)	1.03
6	Ref. 22	σ_{cr} = 40,900(7)	49,800(12)	0.82
7	Ref. 22	σ_{cr} = 47,700(10)	52,500(17)	0.91

* k_s is a buckling load parameter which is proportional to the buckling load, P_{cr} is the total load, lbs., and σ_{cr} is the stress, psi.

From the previous comparisons with existing analytical solutions for isotropic or orthotropically reinforced structural sections and stiffened plates, one can see that the correlations are usually within a few percent. In a few cases where discrepancies are not negligible, possible causes for such deviations are explained. It seems that the existing approximate methods are quite accurate and in most cases should require less computation time in execution than the present method. However, some degrees of uncertainty are always present in such approximate methods which might be due to mode-guessing, less exactness in matching elements, omission of coupling between in-plane displacements and bending loads, etc. In such instances, a more rigorous theory like the present method should be employed.

7. TEST CORRELATIONS WITH BORON REINFORCED PLATES, SECTIONS AND STIFFENED PLATES

Correlations with test data from literature

A. Buckling of axially loaded all-composite laminated flat plates (Refs. 24 and 25)

Four specimens which have simply supported loaded edges are taken from Ref. 24 to correlate with the present theory. The physical properties of boron tape are given in Ref. 24. The test specimens are 20-ply plates and the nominal thickness of boron tape is 0.0053 inch.

Table 7.1 shows test correlations with the present analysis for four plates of size 11 x 9.95 in. with the length 11 in. along the loading direction. Correlations are reasonably good.

Table 7.1 Test Correlations for All-Boron Composite Plates (Ref. 24)

Plate No. in Ref. 26	Condition of Unloaded Sides	Fiber Direction	Buckling Load, N_x, lb/in.			
			Test	Analysis		
				Other Theories	Present Analysis	
					Value	Ratio(test/analysis)
404	free	parallel to load (0°)	199	215* 216**	206.5	0.97
405	free	perpendicular to load (90°)	23.3	23.7* 23.6**	22.6	1.01
404	simple support	parallel to load (0°)	271	292* 299** 285***	286.5	0.95
405	simple support	perpendicular to load (90°)	251	223* 226** 210***	217.0	1.16

* Orthotropic theory
** Rayleigh-Ritz method
***Galerkin method

Good correlation has also been obtained from Ashton and Love's test (Ref. 25). The boron fiber orientation (0° and combinations of 0° and 90°) of the specimens and the buckling load are shown in Table 7.2. The elastic constants of boron and the measured thicknesses of plates that were used in calculations are given in Ref. 25. The results showed that the maximum error is less than 3% for the five cases where load is applied at 0° with respect to fiber orientation and much larger discrepancies for the other five cases where load is applied at 90° to the fiber. Test results were obtained by the Southwell plot. The 90° tests used the same plate after the 0° test was finished by turning the same plate around 90°. The inferior correlations in the cases of 90° specimens may have been caused, as was suggested in Ref. 25, by effects due to boundary constraints. The test specimens are 20-ply square plate measured 10-inches across between edge supports. The loaded edges are clamped and unloaded edges are simply supported.

Table 7.2   Test Correlations for All-Boron Composite Plates (Ref. 25)

Plate No.	Fiber Direction	Load Applied Parallel to 0°*			Load Applied Perpendicular to 0°		
		Test (lbs.)	Present Analysis	Ratio	Test (lbs.)	Present Analysis	Ratio
1	0° - 90° alternate	11,300	11,700	0.97	9,600	9,900	0.97
3	same	9,500	9,170	1.03	9,000	7,700	1.17
4	same	7,400	7,300	1.01	7,200	6,170	1.16
5	all 0°	12,400	12,100	1.02	4,350	3,040	1.43
20	all 0°	13,700	13,350	1.03	4,200	3,360	1.25

*0° refers to the direction of fibers.

Correlations with Boeing's tests of buckling of axially compressed composite reinforced plates, structural sections and stiffened plates

The physical properties used in the analysis are:

Boron-epoxy BF 907

$E_{11} = 29.117 \times 10^6$ psi

$E_{22} = 2.341 \times 10^6$ psi

$G = 0.75 \times 10^6$ psi

$\nu_{12} = 0.2467$

Density = .072 lb/in.^{3}

Titanium 6Al-4V

$E = 16.4 \times 10^6$ psi

$G = 6.2 \times 10^6$ psi   (7.1)

$\nu = 0.3$

Density = 0.158 lb/in.^{3}

38

For boron composite, E_{11} and E_{22} are calculated from a program based on Ref. 26. The G value from the program seemed too high and the present value of 0.75×10^6 is the same as that in Ref. 25. Both E_{22} and G used here are higher than that in Eq. (6.1) which are from Ref. 18.

For aluminum alloy (7075-T6), $E = 10.5 \times 10^6$ psi is used. Elasticity properties of adhesive material which bond composite laminates to the metal base are ignored but its thickness is retained in the analysis.

B. Test correlations of composite reinforced flat plates (Boeing)

Test correlations have been made with recent Boeing tests on composite plates. A total of 48 specimens were tested in which half is symmetrically laminated and the other half is unsymmetrically laminated. The loaded edges are clamped, the unloaded edges are free or simply supported. Measured between clamps and knife-edges, the plate is 9.0 x 2.98 inches. Thickness of the specimen is from 0.097 to 0.127 inches. Details of the geometry are given in the Appendix.

Test results and correlations with analysis are given in Table 7.3. For specimens with unloaded sides free, the calculated buckling load which is for models with simply supported loaded edges is multiplied by a factor of four to get the corresponding value for the clamped-free case. That a factor of four is theoretically correct to be used in the present case is verified numerically by making an analysis of a plate with loaded edges clamped and unloaded sides simply supported and then increase its width to extremity (numerically, from the original 2.98 in. to 500.0 in.). The buckling load of such a wide plate should be almost the same as a clamped-free plate. The result verified that a factor of four to convert the simple-free plate to a corresponding clamped-free plate is numerically correct.

In Table 7.3, errors based on two methods of evaluation are given. Method 1 is based on using the measured length between the clamped edges which is 9.0 inches as the theoretical length of the plate in the analysis. This implies that the test rig is theoretically perfect in making the ends clamped. The average errors for the clamped-simple specimens are 12.7% and 13.6%, and for clamped-free specimens are 19.7% and 38%. Since in the test set-up, the ends of the specimen are clamped between two thick blocks which are then clamped to the testing head, it is possible that perfect clamped conditions might not have been achieved in the tests. If this assumption is true, one may postulate that an end-fixation factor of four used for the clamped-free specimens should be revised. Based on the 24 test results of the clamped-free specimens, an average end-fixation factor is found to be 3.14. Assuming that the buckling load is proportional to the end-fixation factor and inversely proportional to the square of the length of the plate (true for the classical isotropic plate theory), a modified length of 10.15 inches is found ($10.15 = 9 \times (4/3.14)^{1/2}$). Based on this modified length, the errors of correlations are given in Method 2 of Table 7.3. The average errors for the clamped-simple specimens are reduced to 9% and 5.5%; and for the clamped-free specimens, they become 5.9% and 13.5%.

39

Table 7.3 Test Correlations of Symmetrically and
Unsymmetrically Laminated Composite Plates (Boeing)

Test Specimen		Boundary Conditions: Loaded Edges Clamped, Others Simply Supported			Boundary Conditions: Loaded Edges Clamped, Others Free		
		Test, N_x (lbs/in.)	Analysis		Test, N_x (lbs/in.)	Analysis	
			Method 1* Error (%)	Method 2** Error (%)		Method 1* Error (%)	Method 2** Error (%)
Unsymmetrically Laminated	8A-1	3,900	− 0.07	4.0	675	−22.1	4.0
	-2	3,955	− 1.7	4.6	692	−21.4	4.6
	-3	3,020	−11.7	21.6	733	+ 0.1	21.6
	8B-1	3,690	−14.6	3.2	751	−23.0	3.2
	-2	3,825	−13.5	0.6	751	−26.2	0.6
	-3	3,360	−22.5	5.5	751	−20.4	5.5
	8C-1	3,690	− 4.8	7.0	725	−18.1	7.0
	-2	3,290	−14.3	7.7	711	−17.6	7.7
	-3	2,750	−36.6	5.0	691	−21.0	5.0
	8D-1	4,300	− 5.6	5.5	835	−20.2	5.5
	-2	4,100	−13.4	4.1	847	−21.8	4.1
	-3	4,100	−13.4	2.4	832	−24.0	2.4
Average error			−12.7%	+9.07%	Average error |19.7%|***	+5.93%
Symmetrically Laminated	8E-1	3,830	−10.5	− 0.1	1,340	−13.4	11.7
	-2	4,025	−12.6	− 2.1	1,140	−43.2	−12.6
	-3	3,560	−27.4	−15.5	1,010	−61.6	−27.0
	8F-1	5,280	− 4.1	7.1	1,230	−53.5	−20.7
	-2	3,840	−32.8	−18.3	1,310	−32.8	− 4.3
	-3	4,070	−22.9	− 9.3	1,410	−20.9	5.0
	8G-1	5,175	− 7.7	3.4	1,110	−66.1	−31.0
	-2	4,740	−13.6	− 2.1	1,110	−60.0	−25.7
	-3	4,470	− 6.3	4.2	1,140	−36.1	− 6.9
	8H-1	3,960	− 9.2	− 2.1	940	−26.8	− 0.3
	-2	4,260	− 7.6	− 0.2	970	−32.4	− 4.2
	-3	4,025	− 9.0	− 1.8	1,095	−10.7	12.7
Average error			−13.6%	|5.52%|	Average error	−38.1%	|13.5%|

*Method 1 used the measured length between the clamped edges which is 9.0 inches
as the length of the plate in the analysis. Error = 1 − (Analytic result/Test).

**Method 2 used the modified length which is calculated as 10.15 inches in the
analysis. Error = 1 − (Analytic result/Test).

***Average of the absolute values of the errors.

The considerable discrepancy between test and analysis shown in
Table 7.3 may be caused by (1) the constraints provided by the test
setup, (2) the non-uniformity of specimens, and (3) uncertainties in
determining the buckling load from the load-deflection curves. For
item (1), the use of effective length as suggested in Method 2 of
Table 7.3 seemed to have improved the correlations. However, it is
not a satisfactory answer. The non-uniformity in specimens with respect
to the thickness distribution, as indicated in item (2), may cause a
symmetric specimen to become unsymmetric. The effect of eccentricity
on the buckling load will be less severe for plates with sides simply
supported than those with sides free because the latter has no support
from the free sides to resist in-plane bending moments produced by
the eccentricity. In item (3), which appeared in some test results,
it is difficult to determine the buckling load from the longitudinal
load-deflection curve. Two examples which showed such undeterminable
curves are given in the Appendix together with the Southwell plot which
used the lateral load-deflection curve to determine the buckling load.

C. **Test correlations of Boeing specimens of composite reinforced struc-**
   tural sections (Fig. 7.1)
   .   Figure 7.1 shows the geometries of some structural sections, including
angles, Zee's, hat-sections and Tee-sections, reinforced with uni-direc-
tional boron strips and rods. These section specimens, as well as the
specimens of stiffened panels to be described in (7, D.) are machined
flat at the loaded edges, and placed in the testing machine without any
mechanical fastening between the specimen and the testing machine. The
unloaded edges of the section are free. In the analysis, the lips of
Zee-sections and the tips of Tee-sections are idealized as beams while
all the other reinforced parts are treated as plate elements. The
junction of the machined Tee-section of configurations 9I-1 and 9J-1
has been treated as the nodal line of three plate elements without the
fillet and also treated as a beam element with the fillet considered
and joined by three plate elements. The difference in the results
obtained by the two different idealizations was found to be small.

The test results and correlations with analysis are given in Table 7.4.
It can be seen that all correlations are reasonably good except 9A-1 and
9J-1. For specimens of 9A-1, the low prediction might be the result of
idealization which had neglected the corner curvature of the angle-section.
If a curved plate element is added to the present analysis, the quality
of the analysis could be improved. For specimens of 9J-1, the errors
might be caused by difficulties in determining the buckling load from
load-deflection curves of test. It seems that for composite reinforced
plates, there is an initial period of adjustment of a macroscopic nature
in the initial loading stage. As a consequence, in some specimens at
least, the intial part of the load-deflection curve behaves abnormally
and is not dependable. If a specimen is such that its buckling load is
much smaller than the ultimate load, as so happened in the case of 9J-1,
one has difficulty in reading accurately the buckling load from the
test curves.

41

Table 7.4 Test Correlations of Boeing Specimens of Boron-Reinforced Structural Sections (Fig. 7.1)

CONFIGURATION	SPEC. NO.	LENGTH INCH	TEST ULTIMATE LOAD, LBS.	TEST, ELASTIC BUCKLING LOAD, LBS.	AVERAGE	ANALYSIS, BUCKLING PREDICTION LOAD, LBS.	m†	RATIO TEST/ANALY.	REMARK
REINFORCED TITANIUM ANGLE 9A-1	-1 -2 -3 -4	12.0	8,040 8,660 8,380 8,420	3,300 (0.0012)* 3,400 (0.0011) 3,600 (0.0011) 3,700 (0.0015)	3,500	2,390 (0.00051)	1	1.46	Low analytic value is due to neglecting the corner angle of specimen.
	-5 -6 -7	20.0	4,500 6,800 6,600	2,200 (0.00065) 2,000 (0.00050) 2,200 (0.00040)	2,130	2,150 (0.00046)	1	0.99	Better when specimen is longer.
REINFORCED TITANIUM ANGLE 9B-1	-1 -2 -3	15.6	11,240 10,040 9,140	5,800 (4,800)** 6,000	5,900	7,010 (0.00098)	1	0.85	
REINFORCED TITANIUM ZEE 9C-1	-1 -2 -3	13.6	27,700 27,500 26,800	20,000 (0.0028) 17,000 (0.0018) 22,000 (0.0024)	19,700	18,180 (0.0020)	2	1.08	
REINFORCED TITANIUM ZEE 9D-1	-1 -2 -3 -4	12.0	11,240 10,040 9,140 9,260	5,800 (0.0017) 4,800 (0.0011) 5,850 (0.0015) 5,600 (0.0017)	5,510	5,740 (0.00093)	2	0.96	
	-5 -6 -7	20.0	12,200 11,300 11,480	5,600 (0.0014) 5,200 (0.0012) 5,100 (0.0011)	5,300	5,660 (0.00092)	3	0.95	
REINFORCED TITANIUM HAT 9E-1	-1 -2 -3	13.6	32,200 30,500 33,300	32,000 (0.0037) 30,500 (0.0030) 33,300 (0.0033)	33,300	35,890 (0.0057)	1	0.93	-1 and -2 delaminated at the given loads
REINFORCED TITANIUM HAT 9F-1	-1 -2 -3	17.8	6,900	4,300 (0.0020)	4,300	4,390 (0.0016)	3	0.98	-1 tested to 5,840 no failure. -2 debond at 5,700 lbs.
REINFORCED ALUMINUM (FORMED) TEE 9G-1	-1 -2 -3	6.0	20,300 19,080 22,320	17,000 (0.0012) 18,200 (0.0012) not certain	17,620	18,870 (0.0017)	1	0.93	
REINFORCED ALUMINUM (FORMED) TEE 9H-1	-1 -2 -3	6.0	20,940 21,500 22,320	20,940 (0.0066) 21,500 (0.0071) 22,320 (0.0083)	21,520	23,520 (0.0041)	1	0.92	
REINFORCED TITANIUM (MACHINED) TEE 9I-1	-1 -2 -3 -4	10.0	38,000 37,200 38,600 37,000	25,000 (0.0038) 25,000 (0.0037) 26,000 (0.0040) 37,000 (0.0056)	28,250	28,830 (0.0041)	1	0.98	
REINFORCED TITANIUM (MACHINED) TEE 9J-1	-1 -2 -3	9.2	11,040 11,440 10,260	2,200 (0.00087) 3,000 (0.00098) 1,600 (0.00071)	2,270	1,850 (0.00067)	1	1.23	

† Axial half-wave number

% Unit strain, in./in.

** The original test plot of load-vs.-deflection is not available for recheck for the three specimens of 9B-1. The value for specimen -2 is not consistent with the other two specimens and is not included in the average.

D. Tests of Boeing specimens of composite reinforced stiffened plates (Fig. 7.2)

Figure 7.2 shows the geometries of three types of stiffened plates, including composite reinforced hat and angle-section stiffened plates

42

and isotropic honeycomb sandwich plates reinforced internally with boron composite strips. The specimens are machined flat at the ends and placed in the testing machine without any fastenings. The unloaded sides of the panel and stiffeners are free. For long plates, the skin is instrumented for elastic buckling and the skin buckling load is taken for correlation with analysis. For short plates, only ultimate loads were recorded and no analytic correlation will be given. In the analysis, the deep boron reinforcement of the stiffeners in plates -A, -B, -G, -H, -I and -J is treated as beams connected to the two sides of angles as plate elements while in -C, -D, -E and -F, the boron strips together with the immediate skins are treated as plate elements.

From Table 7.5, it can be seen that all the predicted elastic buckling loads are lower than the test ultimate loads, except specimens -E and -F, which are honeycomb sandwich plates whose core was crushed before buckling occurs, and specimen -I where the two numbers are extremely close. The polyimide coat seemed greatly strengthened the buckling strength of the skin in specimen -I. In general, the correlations are satisfactory. The higher predictions are due, at least in part, to the fact that the skin between stiffeners are supported laterally only by frictions developed during the test while in the theory simple support of the skin is assumed.

Table 7.5 Test Correlations of Boeing Specimens of Boron-Reinforced Stiffened Plates (Fig. 7.2)

PART NO.	DESCRIPTION	LENGTH INCH	TEST ULTIMATE LOAD, KIPS	TEST, ELASTIC BUCKLING LOAD, KIPS	ANALYSIS, BUCKLING PREDICTION		
					LOAD, KIPS	m[†]	TEST/ANALYSIS
11-A	REINFORCED ALUMINUM ANGLE, LONG PLATE	33.7	180 (0.0048)[*]	129 (0.0028) skin buckled	150.8 (0.0033)	12	0.85
11-B	REINFORCED ALUMINUM ANGLE, SHORT PLATE	15.0	210 (0.0056)	N. A.[**]	154.1 (0.0033)	6	
11-C	REINFORCED TITANIUM HAT, LONG PLATE	33.7	155 (0.0052)	skin buckled between 25 and 50 kips. Take 30 kips for correlation.	33.5 (0.00088)	14	0.90
11-D	REINFORCED TITANIUM HAT, SHORT PLATE	15.0	181 (0.0061)	N. A.	33.8 (0.00089)	6	
11-E	REINFORCED TITANIUM HONEYCOMB SANDWICH, LONG PLATE	33.7	111 (0.0028)	core crushed	150.4 (0.0038)	1	
11-F	REINFORCED TITANIUM HONEYCOMB SANDWICH, SHORT PLATE	15.0	211 (0.0056)	core failure	200.5 (0.0051)	1	
11-G	REINFORCED TITANIUM ANGLE, LONG PLATE	33.7	356 (0.0043)	257 (0.0032) skin buckled	343.4 (0.0038)	12	0.75
11-H	REINFORCED TITANIUM ANGLE, SHORT PLATE	15.0	461 (0.0056)	N. A.	345.9 (0.0038)	5	
11-I	REINFORCED TITANIUM ANGLE, LONG PLATE (POLYIMIDE COATED)	33.7	350 (0.0042)	325 (0.0026) skin buckled	351.4 (0.0038)	12	0.93
11-J	REINFORCED TITANIUM ANGLE, SHORT PLATE (POLYIMIDE COATED)	15.0	232 (0.0028)	N. A.	349.9 (0.0039)	6	

[†] Axial half-wave number

[*] Unit strain, in./in.

[**] The short specimens were instrumented for crippling; data of skin buckling was not available.

8. DISCUSSIONS
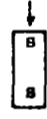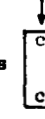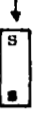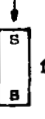
Some points of interest that came up during the numerical study of the method will be discussed in the following.

A. Effect of layer arrangement of composite reinforced plates

A simple calculation which shows the effect of lamina configuration on relative strength and weight of a plate under axial compression is shown in Table 8.1.

For the four boundary conditions studied, the favorable layer arrangement, except the free-free case, is to place composite laminates between metal layers. In such configuration, weight ratio is 73% while strength ratio is 95% in comparison with the all-titanium plate. When the composite is placed outside, strength ratio is dropped to about 50%. A possible explanation is that when the axially compressed plate is buckled, its outer elements farther away from the mid-plane are subjected to more severe extensional and twisting strains than the elements which are closer to the mid-plane and, consequently, adequate face layers should have high G and E_{22} values as well as E_{11} value. For the center layer, since most of its deformation is relatively of the axial extensional type, its E_{11} may be more influential to affect the strength of the plate than its E_{22} and G. This may also explain the low strength ratio of plate No. 4 in Table 8.1, since in that case the composites in one side of the face of the plate still subjected to twisting in buckling deformation.

Table 8.1 Uniaxial Compressive Buckling of Laminated Plates
(all 0° fiber) with Various Thickness Ratios

No.	Plate 9" x 2.8"	Relative Weight	Buckling Load Ratio			
1	▭ 0.10	1.0	1.0 ($\bar{N}_{11}$=7553 lb/in.)	1.0 ($\bar{N}_{11}$=7554)	1.0 ($\bar{N}_{11}$=968)	1.0 ($\bar{N}_{11}$=168)
2	.1 ▤ .025 / .025	0.728	0.941	0.964	0.936	1.130
3	.1 ▤ .025 / .025	0.728	0.459	0.564	0.554	1.928
4	.1 ▤ .05 / .05	0.728	0.526	0.565	0.532	1.387
5	▨ 0.10	0.456	0.328	0.466	0.490	2.06

Titanium / Composite

s: simply supported   c: clamped   f: free

B. **Effect of in-plane constraints along the unloaded sides of a stiffened plate**

The effect of in-plane displacements along the unloaded sides of a stiffened plate can be seen from a calculation made for the single stiffener plate of Fig. 6.2. In the related reference[18], the in-plane constraints at the two sides are $N_{12} = N_{22} = 0$ where N_{12} is the shear force. If the condition $N_{12} = 0$ is replaced by $u = 0$ which means the displacement in the shear force direction is prevented instead of the shear force itself, the present analysis shows that the buckling load will be increased considerably. Table 8.2 gives the values.

Table 8.2 Effects of In-Plane Constraints at the
Unloaded Sides and Different Stiffener Idealization
for the Stiffened Plate of Fig. 6.2

β Value in Fig. 6.2	In-Plane Boundary Constraints	Stiffener Idealization	Relative Buckling Load
2	$N_{22} = N_{12} = 0$	as beam (Ref. 18)	1.00 ($N/N_{eq} = 0.93$)*
	$N_{22} = N_{12} = 0$	as beam	1.00
	$N_{22} = u = 0$	as beam } (present analysis)	1.24
	$N_{22} = u = 0$	as plate	1.54
8	$N_{22} = N_{12} = 0$	as beam (Ref. 18)	1.00 ($N/N_{eq} = 2.86$)*
	$N_{22} = N_{12} = 0$	as beam	1.00
	$N_{22} = u = 0$	as beam } (present analysis)	1.23
	$N_{22} = u = 0$	as plate	1.32

*$E_s A_s / Ebt = 1.5$, see Fig. 6.2

It can be seen that for the prescribed geometry, buckling strength is increased more than 20% by preventing the sides from moving in the direction of the load. For different geometry, however, the effect may not be so noticeable.

C. **Difference due to idealization of stiffeners and flanges**

Stiffeners and flanges of a section or a stiffened plate can be idealized into either beam elements or plate elements depending on the geometry of the member itself and the geometry of the structure. However, different ways of idealization may produce quite substantial discrepancies in the analytical results. Table 8.2 above shows the difference in loads by treating the single stiffener in Fig. 6.2 first as a beam and then as a plate. Two similar instances are shown in Table 8.3 taken from structures of Figs. 6.1 and 6.4.

Table 8.3 Effect of Different Ways of
Idealization of Stiffeners and Flanges

Example Descriptions	Stiffener or Flange Idealization	Buckling Load
Web with orthotropic flange. Long-wave mode described in Sec. (6, A) and Fig. 6.1	flange as beam (Ref. 18)	k_w = 1.56
	flange as beam (present analysis)	1.58
	flange as plate (present analysis)	5.90
Plate stiffened by six isotropic integral stiffeners. Long-wave mode described in Sect. (6, C) and Fig. 6.4, panel 1.	stiffeners as beams (Ref. 20)	P_{cr} = 23,450 lbs
	stiffeners as beams (present analysis)	22,347
	stiffeners as plates (present analysis)	29,468

Such large discrepancy as shown in the first example of Table 8.2 in treating the flange as beam and as plate warrants further study of the matter.

D. Buckling mode shape plots

In Fig. 6.5, the mode shapes of a truss core sandwich panel corresponding to two different core web thicknesses have been shown. Such plots yield valuable physical insight into the instability mechanisms of structures. An additional example is given here to demonstrate the usefulness of such mode shape plot in identifying weak members in a structure from a buckling point of view. Fig. 8.1.a shows the buckling mode shape for panel 1 in Fig. 6.4, with three stiffeners. It is seen that the stiffener is weaker than the skin from the point of view of buckling. In the succeeding figures of Fig. 8.1, the stiffener thickness is gradually increased and the skin thickness correspondingly decreased so that the total cross-sectional area (and hence the weight) is the same in all cases. It is seen that, for the same weight, the panel of Fig. 8.1.c carries the maximum load, a gain of 54% over the panel of Fig. 8.1.a. Similar studies can be made on more complicated cross-sections. The usefulness of the mode shape plot in assisting design and in structural optimization is evident.

9. CONCLUSIONS

The present analysis for the instability of composite plates, sections and stiffened plates with composite reinforcement, is an exact theory in the classical sense. The connection between plate elements and between plate and beam elements, with the effect of offset included in the analysis, and the considerations for the conditions at all the unloaded edges of the structure are rigorous and consistent with the linear plate theory and elementary beam theory.

Reasonably good agreement with existing analytical and test data is obtained from the results of the correlation study. Some scattering in test correlations indicates the degree of uncertainties in dealing with composite materials in theory as well as in techniques of fabrication of the composite reinforced stiffened structures. If the composites are so ideal such that no shear strain exists in the direction of the thickness, all layers are homogeneously orthotropic, the material stress-strain follows linear Hooke's law until buckling occurs, no residual stress, no sliding between layers and no separation occurs between laminates and metal, then the mathematical model stipulated for laminated composites in the analysis is exact in reality, and reasonable correlation between theory and tests might be expected. Further complication arises from the uncertain properties of the adhesive layer which bond the composite lamina to the metal. When the thickness of the adhesive layer is of comparable order of magnitude as the thickness of the composites, it could be important to include the elasticity of the adhesive layer and the effect of the inter-lamina shear into the analysis.

Since the present method combines local instability, which involves only some of the elements, as well as general instability, which involves the whole structure, the solution of the eigenvector for the particular eigenvalue (buckling load) is useful. This eigenvector capability has been included and it would be useful in an optimization analysis where the weak members which buckled first could be detected and reinforced.

The present method could be used in conjunction with existing optimization and direct-search programs to establish minimum-weight configuration for panels with composite reinforced stiffeners.

REFERENCES

1. Ramberg, W., and Levy, S., "Instability of Extrusions under Compressive Loads," Journal of the Aeronautical Sc., October 1945.

2. Goodman, S., and Boyd, E., "Instability of Outstanding Flanges Simply Supported at One Edge and Reinforced by Bulbs at Other Edge," TN-1433, 1947, NACA.

3. Goodman, S., "Elastic Buckling of Outstanding Flanges Clamped at One Edge and Reinforced by Bulbs at Other Edge," TN-1985, 1949, NACA.

4. Hu, P. C., and McCulloch, ., "The Local Buckling Strength of Lipped Z-Columns with Small Lip Width," TN-1335, 1947, NACA.

5. Wittrick, W. H., "A Unified Approach to the Initial Buckling of Stiffened Panels in Compression," The Aeronautical Quarterly, August 1968, pp. 265-283.

6. Stowell, E. Z., "Compressive Strength of Flanges," Report 1029, 1949, NACA.

7. Chilver, A. H., "A Generalized Approach to the Local Instability of Certain Thin-Walled Struts," The Aeronautical Quarterly, Vol. IV, August 1953, pp. 245-260.

8. Goldberg, J. H., Bogdanoff, J. L., and Glauz, W. D., "Lateral and Torsional Buckling of Thin-Walled Beams," IABSE Publications, Vol. 24, 1964, pp. 91-100.

9. Bulson, P. S., "Local Instability Problems of Light Alloy Struts," Research Report No. 29, The Aluminum Development Association, London, December 1955.

10. Bulson, P. S., "Local Stability and Strength of Structural Sections," Thin-Walled Structures, edited by A. H. Chilver, published by Chatto & Windns, London, 1967.

11. Bulson, P. S., "The Local Instability of Structural Sections with Flange Reinforcements," Thin-Walled Steel Structures, edited by R. C. Rockey, Grosby and Lockwood, London, 1969.

12. Grobarah, A. A., and Tso, W. K., "Overall and Local Buckling of Channel Columns," Journal of the Eng. Mech. Div., Proceedings of ASCE, April, 1969, pp. 447-462.

13. Tsai, S. W., "Strength Characteristics of Composite Materials," CR-224, April 1965, NASA.

14. Ashton, J. E., Halpin, J. C., and Petit, P. E., **Primer on Composite Materials: Analysis**, Progress in Material Sc. Series Vol. III, Technical Publication Co., Stamford, Connecticut, 1969.

15. Oeverli, V. and Viswanathan, A. V., (a) BUCLAP - A Computer Program for Uniaxial Compressive Buckling Loads of Orthotropic Laminated Plates. NASA CR-111869, 1971. (b) BUCLAS - A Computer Program for Uniaxial Compressive Buckling Loads of Orthotropic Laminated Structural Sections. NASA CR-111870, 1971. (c) BUCLASP - A Computer Program for Uniaxial Compressive Buckling Loads of Orthotropic Laminated Stiffened Plates. NASA CR-111871, 1971.

16. Argyris, J. H., and Dunne, P. C., Structural Principles and Data, edited by D. M. A. Leggett and M. Langley, 1934, Pitman Press, London.

17. Roark, R. J., "Formulas for Stress and Strain," 4th Ed. 1965, McGraw-Hill Book Company.

18. Peterson, J. P., "Structural Efficiency of Aluminum Multiweb Beams and Z-Stiffened Panels Reinforced with Filamentary Boron-Epoxy Composite," TN D-5856, June 1970, NASA; also presented at the AIAA/ASME 11th Structures, Structural Dynamics and Materials Conf., April 1970, Denver, Colorado.

19. Becker, H., "Handbook of Structural Stability," Part II, TN-3782, July 1957, NACA.

20. Block, David L., Card, Michael F., and Mikulas Jr., Martin M., "Buckling of Eccentrically Stiffened Orothtropic Cylinders," TN D-2960, August 1965, NASA, eq. (A3), p. 23.

21. Anderson, Melvin S., "Local Instability of the Elements of a Truss-Core Sandwich Plate," TR R-30, 1959, NASA, Figure 5(a), p. 6.

22. Engineering Sciences Data, 01.01.18 and 01.01.20, Engineering Sciences Data Unit, Royal Aeronautical Society, London.

23. Pride, Richard A., Royster, Dick M., and Gardner, James E., "Influence of Various Fabrication Methods on the Compressive Strength of Titanium Skin-Stringer Panels," TND-5389, NASA, August 1969.

24. Mandell, J. F., "An Experimental Investigation of the Buckling of Anisotropic Fiber Reinforced Plastic Plates," AFML-TR-68-281, October 1968, Air Force Materials Laboratory, Air Force Systems Command, Wright-Patterson Air Force Base, Ohio.

25. Ashton, J. E., and Love, T. S., "Experimental Study of the Stability of Composite Plates," Journal of Composite Materials, Vol. 3, April 1969, p. 230.

26. Tsai, S. W., "Structural Behavior of Composite Materials," CR-71, July 1964, NASA.
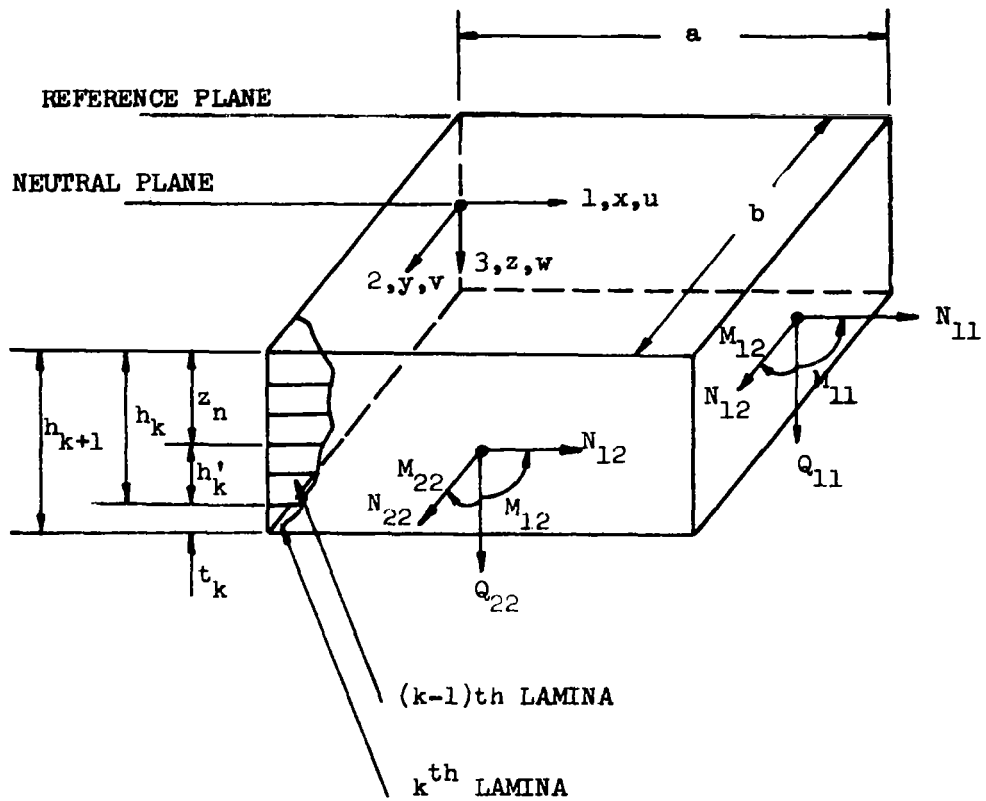
Fig. 4.1 Sign conventions for flat laminated plate
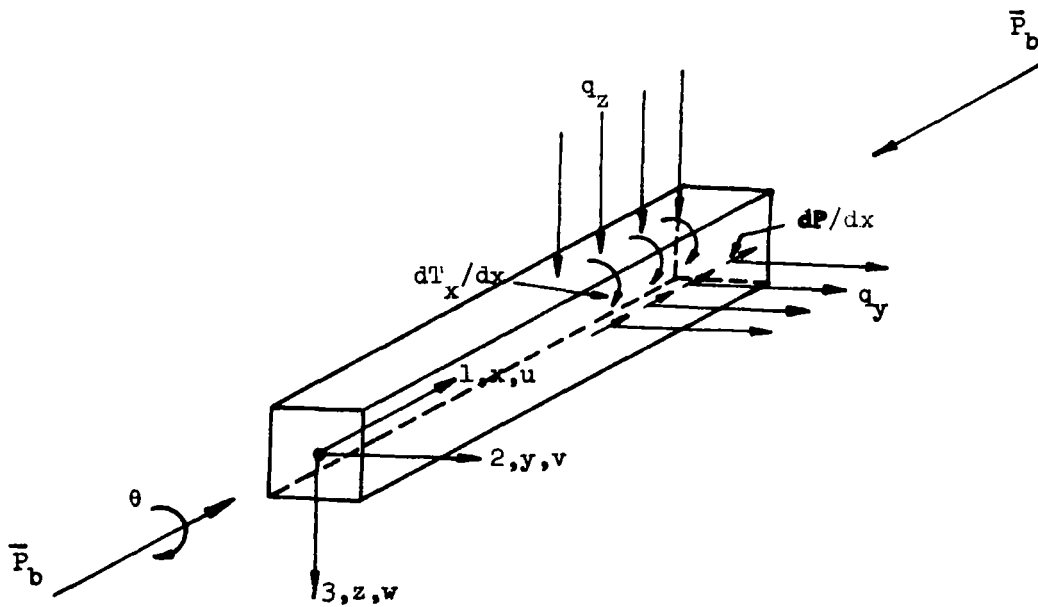
Fig. 4.2 Beam element forces and displacements
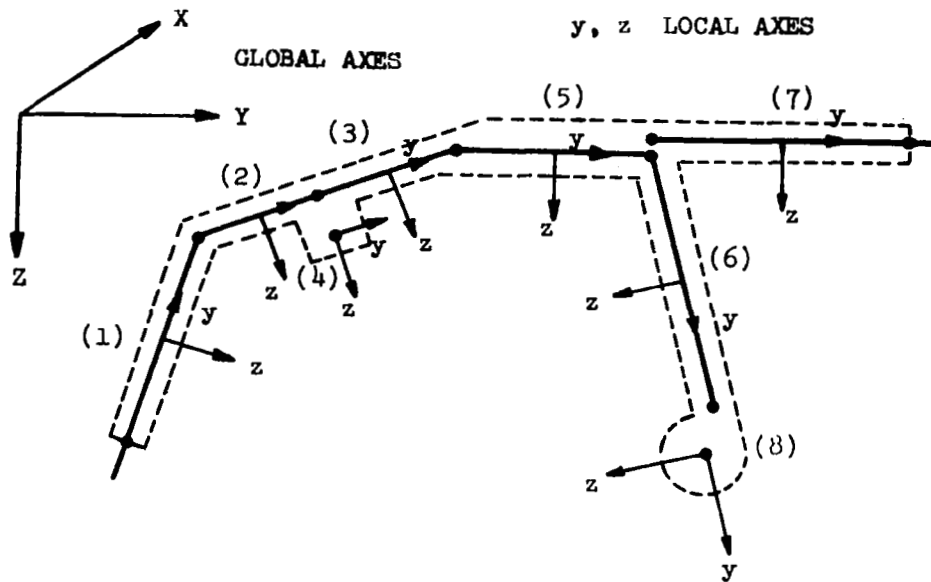
Fig. 5.1 Idealization and axes systems of an arbitrary section
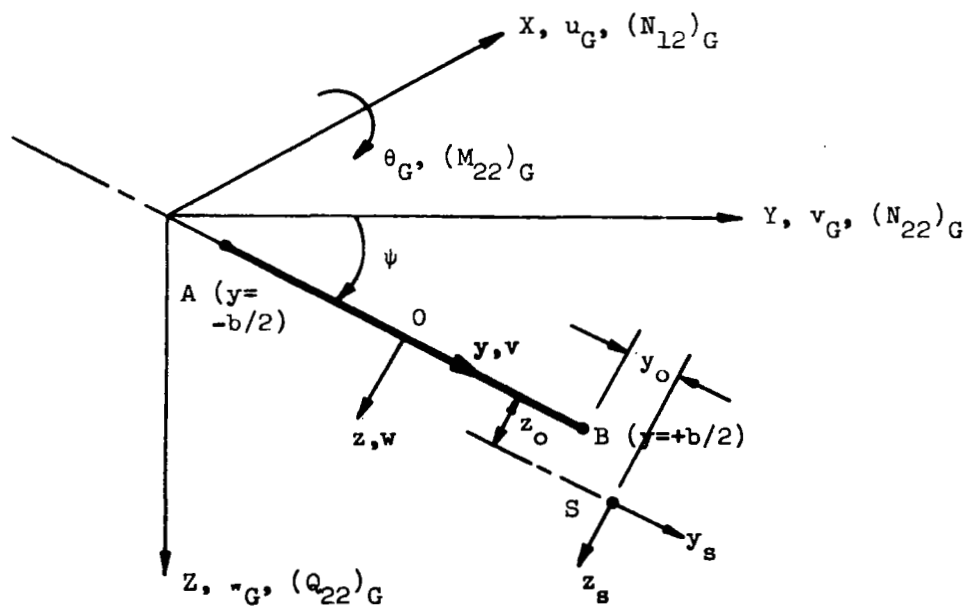of a structural section or stiffened plate

Fig. 5.2 Global coordinates and sign convention of flat plate element
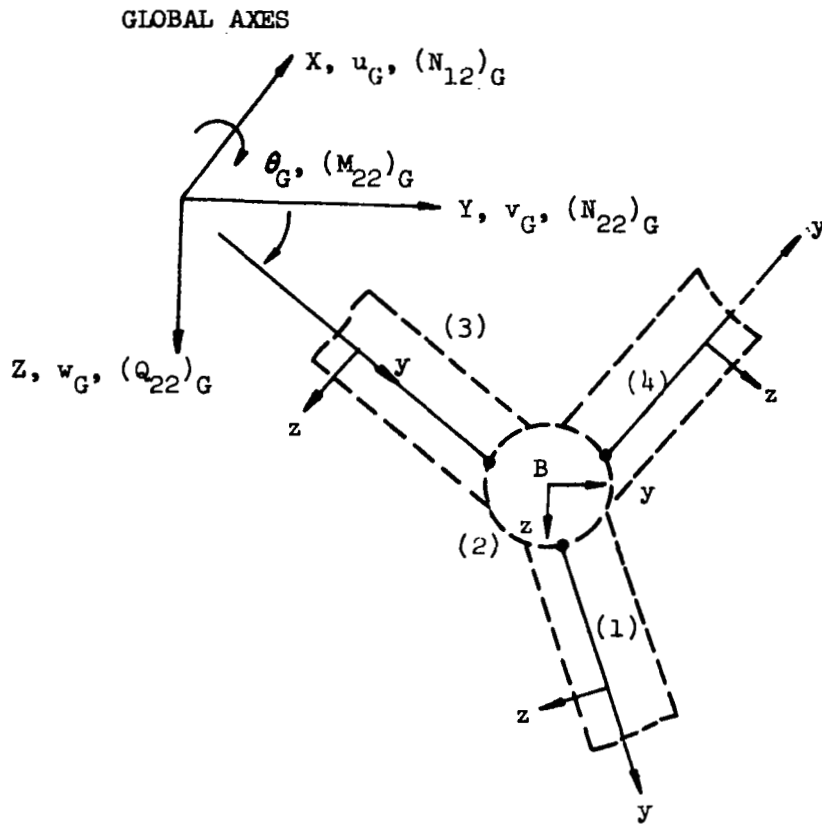
51

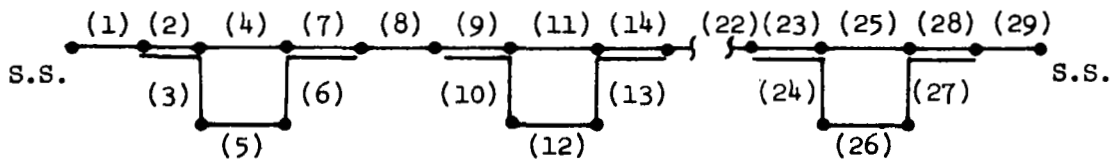Fig. 5.3 A joint where three plate elements meet
a beam element

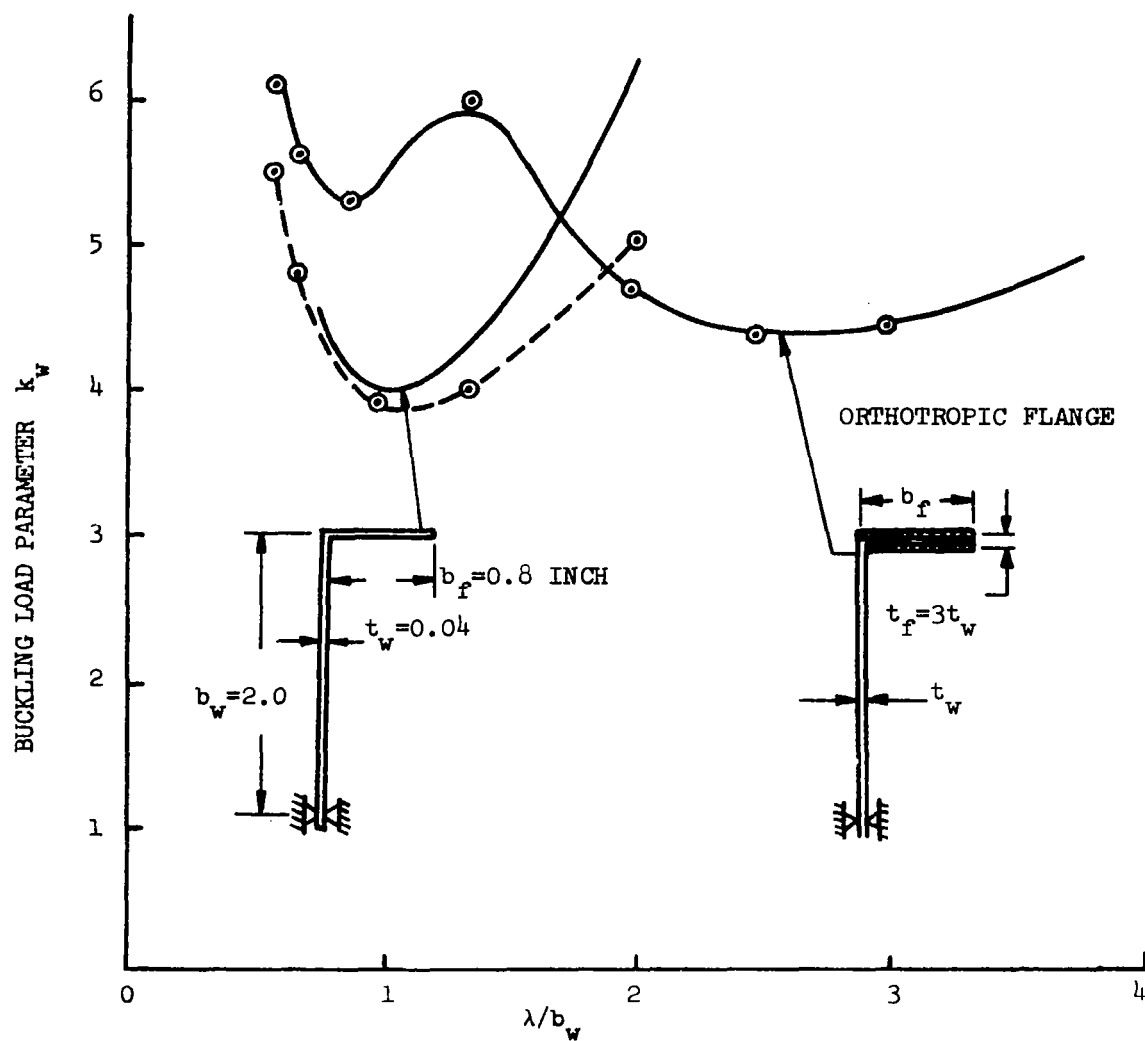Fig. 5.4 A hat-section stiffened plate with four
hat-sections

52

Fig. 6.1 Buckling of web-flange with and without composite
reinforcement at the flange (Ref. 18)

———— analytical results from Ref. 18

⊙ results from present method

λ = axial half-wave buckle length

$k_w = \bar{N}_x b_w^2 / \pi^2 D_w$ where $\bar{N}_x$ = load per inch on web

D_w = bending stiffness of web
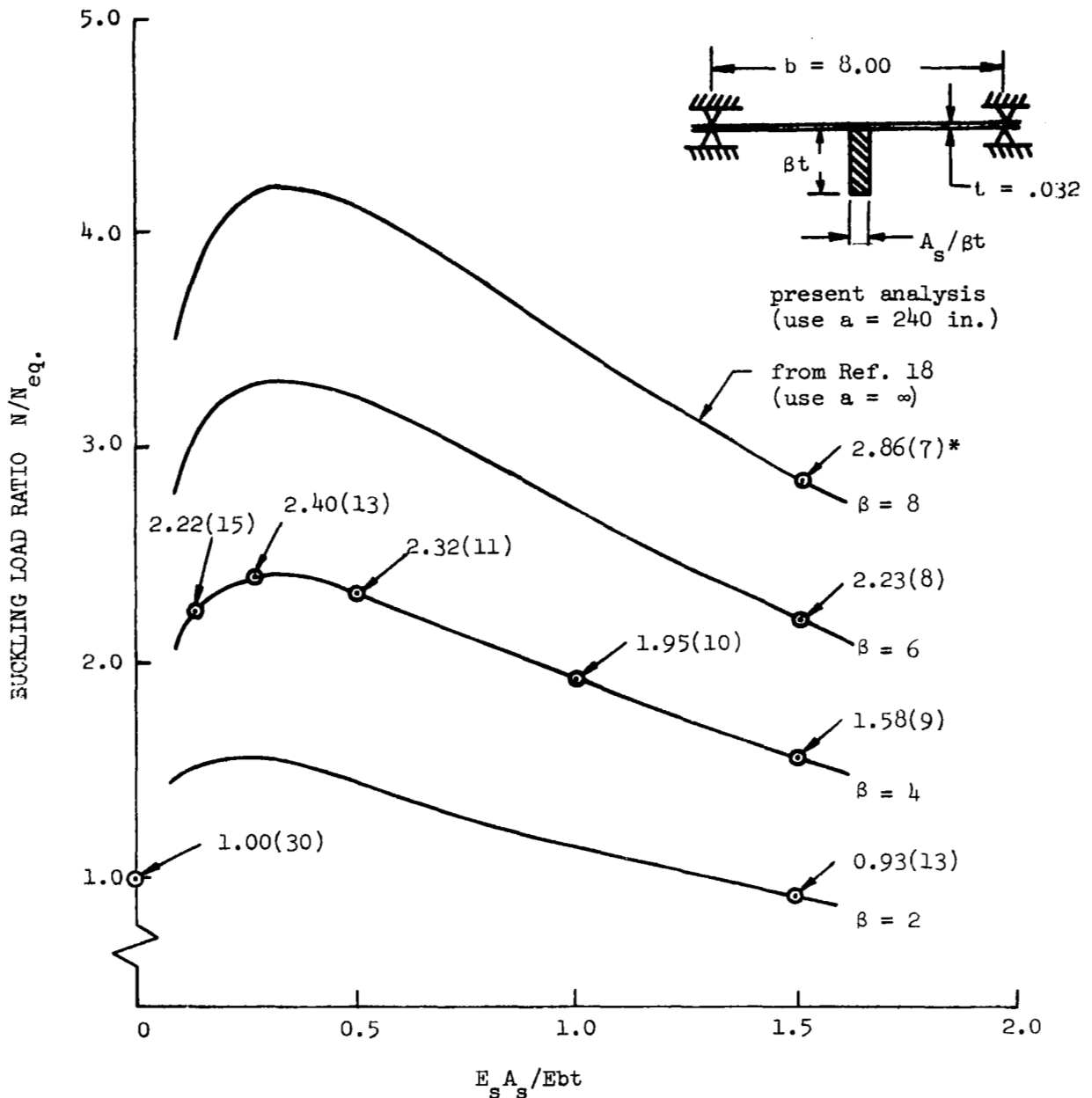
Fig. 6.2 Discretely stiffened isotropic plate buckled under axial
compression – single shallow eccentric stiffener (Ref. 18)

E_s = Young's modulus of stiffener; E = same for plate

A_s = cross sectional area of stiffener

N = load per inch on plate, including stiffener load

$N_{eq.}$ = buckling load per inch on an equivalent plate of equal
weight with constant thickness

*axial half-wave number
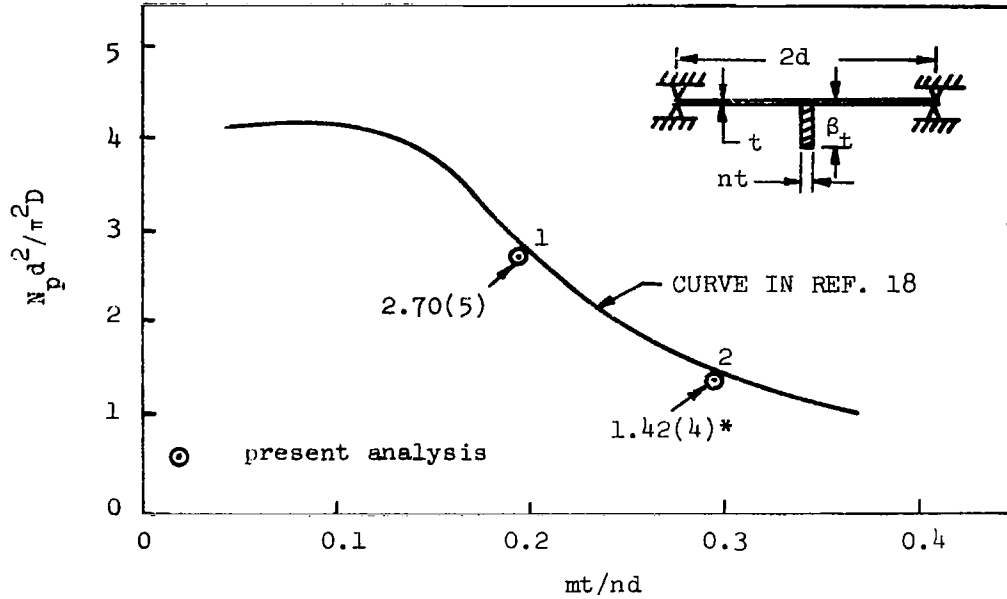
Fig. 6.3 Discretely stiffened plate – single eccentric
orthotropic deep stiffener (Ref. 18)

* number of axial half-wave

N_p = load per inch on isotropic plate

D = bending stiffness of plate

Geometry at points 1 and 2 on Fig. 6.3: (unit: inch)

Point	d	t	β	n	a = length of plate
1	3.0	.048	25.0	2	30.0
2	4.0	.032	75.0	2	40.0

1		Al. alloy. 6 stiffeners $a = 12.3$ $t_s = 0.089$ $b_s = 2.05$ $t_w = 0.058$ $b_w = 1.06$ $a =$ length of plate
2		Al. alloy. 6 stiffeners $a = 15.0$ $t_s = 0.080$ $t_f = t_w$ $b_s = 3.0$ $t_w = 0.056$ $b_w = 1.8$ $b_f = 0.54$
3		Al. alloy. 6 stiffeners |	a	$t_w = t_f$	b_w	b_f
---	---	---	---	---
A	14.4	.04	1.92	.576
B	14.4	.04	0.96	.288
C	16.0	.048	1.50	.500	
4		Al. alloy. 13 60°-cells $a = 6.0$ $t_c = 0.02$ for case A $b_s = 1.0$ $= 0.01$ for case B $t_f = 0.02$
5		Al. alloy. 7 cells $a = 8.96$ $b_{f1} = 2.56$ $b_c = 1.06$ $b_{f2} = 1.06$ $t_c = .036$ $t_f = .048$
6		Al. alloy. 6 stiffeners $a = 16.0$ $b_f = 0.500$ $b_w = 1.436$ $t_s = 0.080$ $b_s = 1.876$ $t_w = t_f = 0.048$
7		Al. alloy. 5 stiffeners $a = 20.0$ $b_s = 1.5$ $b_{f1} = 0.5$ $b_w = 1.436$ $b_{f2} = 1.2$ $t_w = t_{f1} = t_{f2} = .048$

Fig. 6.4   Geometry of seven types of isotropically stiffened plates and sandwich panels for analytical correlations (unit: inch)
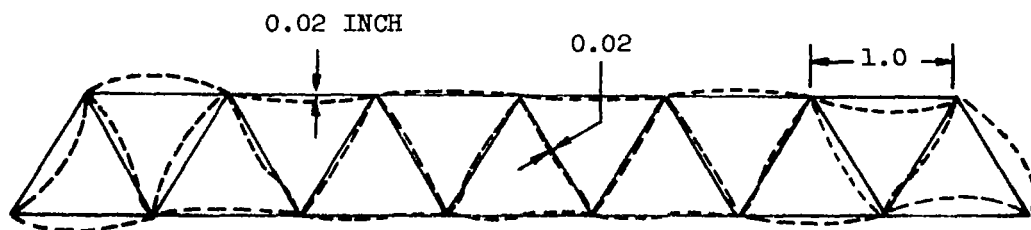
Case A of Panel 4 in Fig. 6.4.   Core-restrains-face type
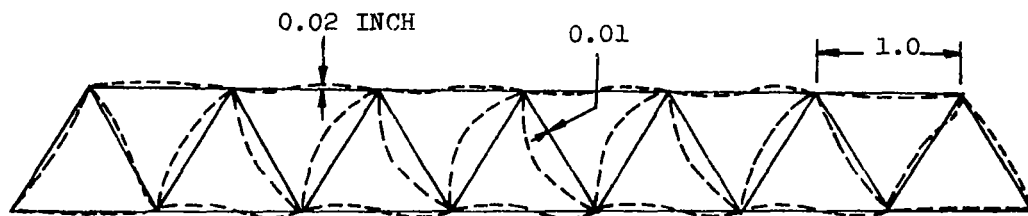
Case B of Panel 4 in Fig. 6.4.   Face-restrains-core type

Fig. 6.5   Buckling shapes of a truss-core sandwich panel

Case A: Core-restrains-face type
(Core web thickness = 0.2)

Case B: Face-restrains-core type
(Core web thickness = 0.01)

Note: The relative amplitude of each element
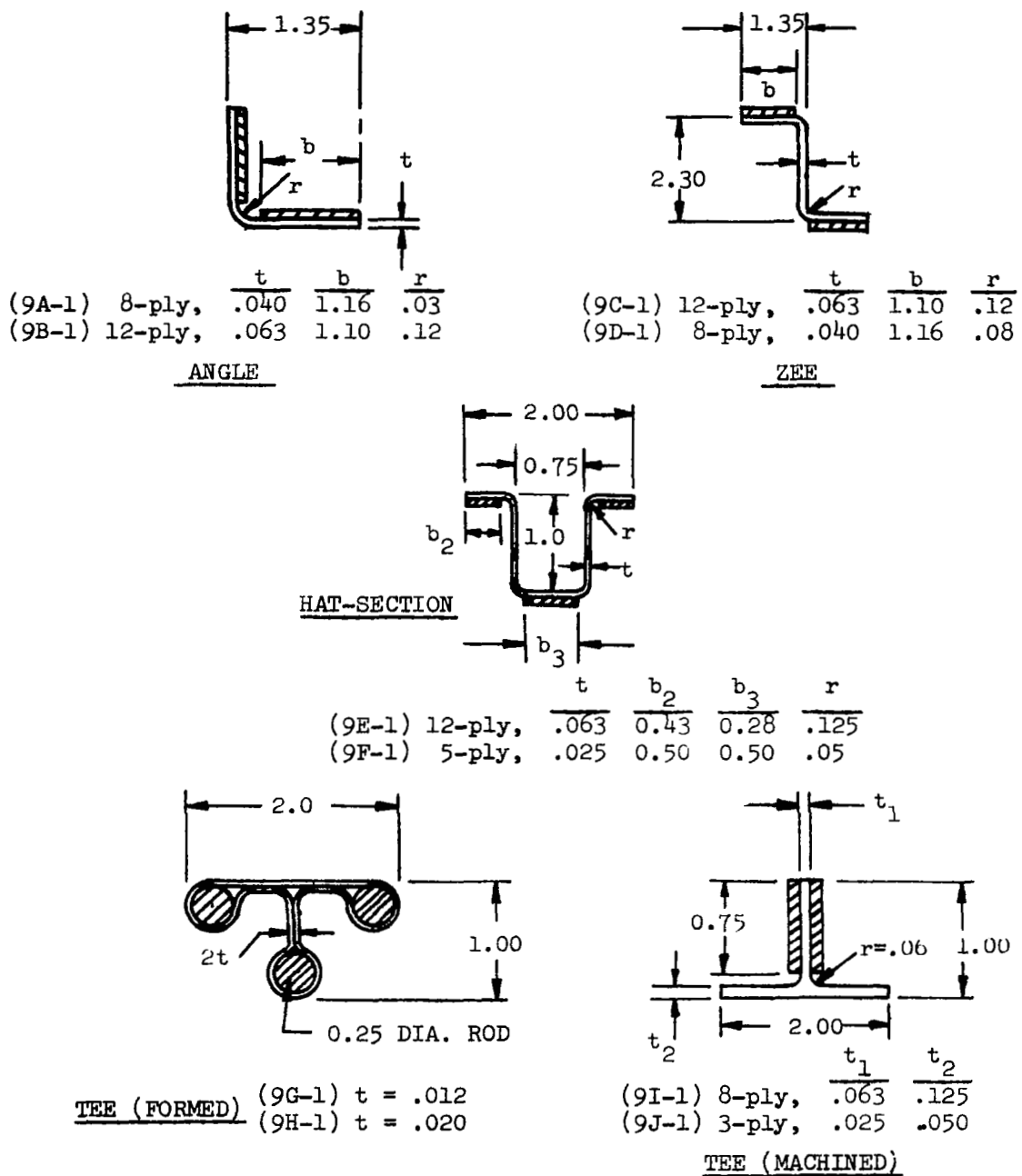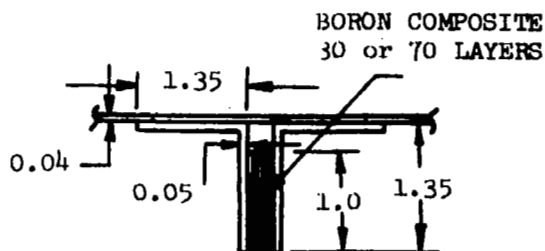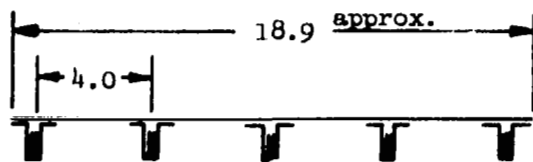of the buckled shape is drawn in scale

57

Fig. 7.1 Geometry of test specimens of boron-reinforced titanium or aluminum alloy structural sections.

Materials given in Table 7.4. Ply thickness of boron tape = 0.0053 inch (nominal). Adhesive thickness = 0.018 approx.
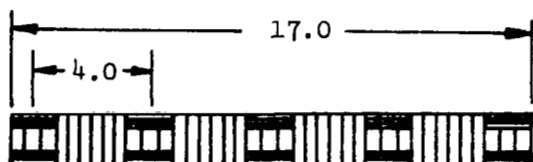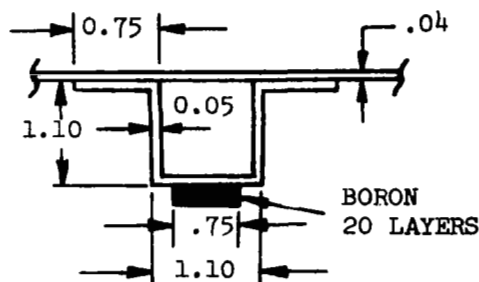
⊏⊐ metal   ▨ boron composite layers

58

Panels 11-A, -B. Al. alloy skin and stiffeners, 30 layers composite
Panels 11-G, -H, -I, -J. Titanium skin and stiffeners, 70 layers
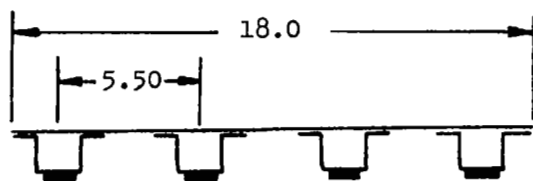
Panels 11-C, -D. Titanium skin
and stiffeners

Panels 11-E, -F, Titanium skin
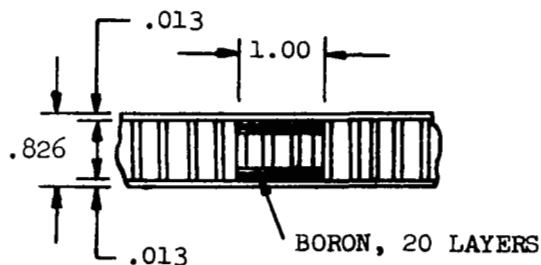and stiffeners

Fig. 7.2   Geometry of test specimens for composite reinforced
stiffened plates and stiffened honeycomb-sandwich panel
(Unit: inch)
Thickness of each boron tape layer = 0.0053 in.
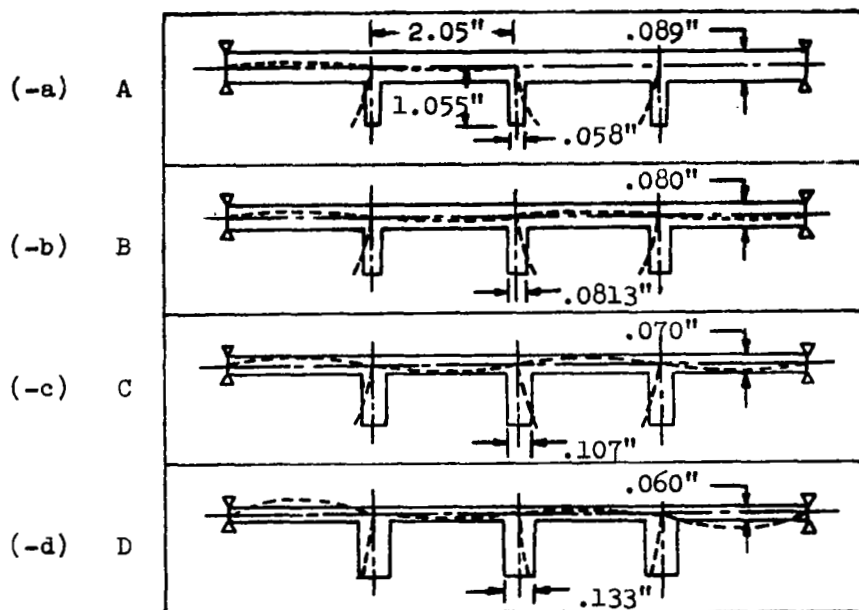Thickness of adhesive layer = 0.013 approx.

Fig. 8.1 Buckling mode shape plots of a three-stiffener plate (amplitude drawn in correct relative magnitude)

Buckling Data

Configuration	Buckling type	P_{cr}, lbs.	m	ε_{cr}, in./in.
A	Stiffener buckled	27,540	6	0.00317
B	Stiffener buckled	38,346	5	0.00420
C	Skin and Stiffeners buckled	42,491	5	0.00490
D	Skin near edge support buckled	35,285	7	0.00407

Note: All configurations have the same cross sectional area

APPENDIX

SUPPLEMENTARY ANALYSIS,

ANALYTICAL CORRELATIONS AND GEOMETRIC DETAILS

INTRODUCTION

The Appendix of the report contains some peripheral equations which are not essential in the understanding of the analysis but would complement the equations in the main text in working out numerical problems which contain plate elements with uncoupled features ($B_{ij} = 0$). Also included in the Appendix are a few additional analytical correlations and a detailed geometry of the Boeing specimens of composite reinforced plates.

1. EQUATIONS TO IMPLEMENT EQUATIONS IN THE MAIN TEXT

1.1 Equations for Rectangular Composite Plates

In the main text, equations for plates with elastically restrained sides are given in Eqs. (5.1) to (5.10a). For other boundary conditions, corresponding equations are given below.

Plates with all four sides simply supported

Assume that the origin of the axes is placed at a corner of the plate. The boundary conditions are:

x = 0 or a		y = 0 or b	
(i) $w = 0$		(i) $w = 0$	
(ii) $M_{11} = 0$		(ii) $M_{22} = 0$	
(iii) $N_{11} = 0$	(II-1)	(iii) $u = 0$	(II-2)
(iv) $v = 0$		(iv) $N_{22} = 0$	

Displacement functions assumed which automatically satisfy the above conditions are:

$$w = W_{mn} \sin\alpha \sin\beta$$

$$v = V_{mn} \sin\alpha \cos\beta \qquad\qquad (II-3)$$

$$u = U_{mn} \cos\alpha \sin\beta$$

where

$\alpha = m\pi x/a$ and $\beta = n\pi y/b$ and m and n are half-wave numbers.

On substituting the displacement functions in the equilibrium equations, one arrives at an equation similar to Eq. (5.6) from which the buckling load $\bar{N}_{11}$ is obtained explicitly as a function of m and n. Vary m and n, the lowest $\bar{N}_{11}$ thus obtained is the buckling load.

Plates with loaded edges clamped, other two sides simply supported

Assume a coordinate system such that the x-axis coincides with one side of the plate and the y-axis is at the middle. The boundary conditions are:

$x = \pm \frac{a}{2}$		y = 0 or b	
(i) $w = 0$	(II-4)	(i) $w = 0$	(II-5)

(ii) $w_{,x} = 0$ (ii) $M_{22} = 0$

(iii) $N_{11} = 0$ (II-4) (con't)   (iii) $u = 0$ (II-5) (con't)

(iv) $v = 0$ (iv) $N_{22} = 0$

Displacement functions assumed are (upper rows correspond to symmetric mode and lower rows to antisymmetric mode):

$$w = \sum_{i=1}^{4} W_i \begin{pmatrix} \cosh\alpha \\ \sinh\alpha \end{pmatrix} \sin\beta \qquad \alpha = \pi p_i x/a$$

$$v = \sum_{i=1}^{4} V_i \begin{pmatrix} \cosh\alpha \\ \sinh\alpha \end{pmatrix} \cos\beta \qquad \beta = n\pi y/b \qquad (II-6)$$

$$u = \sum_{i=1}^{4} U_i \begin{pmatrix} \sinh\alpha \\ \cosh\alpha \end{pmatrix} \sin\beta$$

which satisfies the boundary conditions at $y = 0$ and b.

Since the displacements satisfy the conditions of symmetry or antisymmetry at the middle of the plate ($x = 0$), only the four conditions at $x = a/2$ need to be considered and only four roots of Eq. (5.6) will be used. The other four, say, the negative roots, will be ignored.

The 4x4 buckling determinant (Eq. (5.10)) for the symmetric axial mode, can be written as

$$\begin{vmatrix} \cosh(\pi p_i/2) & \cdots \\ p_i \sinh(\pi p_i/2) & \cdots \\ [A_{11}L_{2i}(p_i/a)-A_{12}L_{1i}(n/b)-B_{11}(p_i/a)^2+B_{12}(n/b)^2]\cosh(\pi p_i/2) & \cdots \\ L_{1i}\cosh(\pi p_i/2) & \cdots \end{vmatrix} = 0 \qquad (II-7)$$

$$i=1,2,3,4$$

where L_{1i} and L_{2i} are given in Eqs. (5.8). For the antisymmetric mode, one simply changes cosh to sinh and sinh to cosh in the above equation.

When the coupling matrix B_{ij} is zero, it is possible to reduce the buckling determinant to 2x2 since only the first two boundary conditions, (i) and (ii) of Eq. (II-4) need to be enforced.

Plate with loaded edges simply supported, one side simply supported, the other side free

The coordinate axes are the same as the elastically restrained plate. The boundary conditions are:

63

$\underline{x = 0 \text{ or } a}$ $\underline{y = -b/2}$

(i) $w = 0$ (i) $w = 0$

(ii) $M_{11} = 0$ (ii) $M_{22} = 0$

(iii) $N_{11} = 0$ (II-8)   (iii) $u = 0$ (II-9)

(iv) $v = 0$ (iv) $N_{22} = 0$

$$\underline{y = +b/2}$$

(i) $M_{22} = 0$ (iii) $N_{12} = 0$

(ii) $\dfrac{\partial M_{22}}{\partial y} + 2\,\dfrac{\partial M_{12}}{\partial x} = 0$ (iv) $N_{22} = 0$ (II-10)

Displacement functions assumed are the same as Eq. (5.1). Proceeding exactly as before, the resulting 8x8 determinant can be written as

$$
\begin{vmatrix}
\exp(\pi p_i/2)G_{2i} & \cdots \\
\exp(\pi p_i/2)G_{1i} & \cdots \\
\exp(\pi p_i/2)G_{4i} & \cdots \\
\exp(\pi p_i/2)G_{3i} & \cdots \\
\exp(-\pi p_i/2) & \cdots \\
\exp(-\pi p_i/2)G_{5i} & \cdots \\
\exp(-\pi p_i/2)L_{2i} & \cdots \\
\exp(-\pi p_i/2)G_{4i} & \cdots \\
\end{vmatrix} = 0 \qquad\qquad \text{(II-11)}
$$

$$i = 1,2,\ldots 8$$

where L_{1i}, L_{2i} are given in Eq. (5.8), G_{1i} to G_{4i} are given in Eq. (5.10a) and G_{5i} is defined as

$$G_{5i} = -B_{12}(m/a)L_{2i}+B_{22}L_{1i}(p_i/b)+D_{12}(m/a)^2-D_{22}(p_i/b)^2 \qquad \text{(II-12)}$$

When $B_{ij} = 0$, the order of the buckling determinant is reduced to 4x4, since the boundary conditions that need to be enforced are:

$\underline{y = -b/2}$ $\underline{y = +b/2}$

(1) $w = 0$ (1) $M_{22} = 0$

                                                         (II-13)

(2) $M_{22} = 0$ (2) $\dfrac{\partial M_{22}}{\partial y} + 2\,\dfrac{\partial M_{12}}{\partial x} = 0$

<u>Plate with loaded edges simply supported, the other two sides free</u>

The loaded plate has the same coordinate system as the elastically restrained plate. The boundary conditions are:

<u>x = 0 and a</u>   <u>y = ±b/2</u>

(i) $w = 0$ (i) $M_{22} = 0$

(ii) $M_{11} = 0$ (ii) $\dfrac{\partial M_{22}}{\partial y} + 2\,\dfrac{\partial M_{12}}{\partial x} = 0$

(iii) $N_{11} = 0$ (II-14)   (iii) $N_{12} = 0$ (II-15)

(iv) $v = 0$ (iv) $N_{22} = 0$

Displacement functions assumed are (the upper rows correspond to symmetric mode and the lower rows to antisymmetric mode):

$$w = \sum_{i=1}^{4} W_i \binom{\cosh\beta}{\sinh\beta} \sin\alpha \qquad\qquad \alpha = m\pi x/a$$

$$v = \sum_{i=1}^{4} V_i \binom{\sinh\beta}{\cosh\beta} \sin\alpha \qquad\qquad \beta = \pi p_i y/b \qquad (II-16)$$

$$u = \sum_{i=1}^{4} U_i \binom{\cosh\beta}{\sinh\beta} \cos\alpha$$

The buckling determinant is formed from the enforced boundary conditions (Eq. (II-15)) using the four positive p_i roots from Eq. (5.6). The resulting 4x4 buckling determinant is (for the symmetric mode)

$$\begin{vmatrix} \cosh(\pi p_i/2)G_{5i} & \cdots \\ \sinh(\pi p_i/2)G_{1i} & \cdots \\ \cosh(\pi p_i/2)G_{4i} & \cdots \\ \sinh(\pi p_i/2)G_{3i} & \cdots \quad {\scriptstyle i=1,2,3,4} \end{vmatrix} = 0 \qquad (II-17)$$

where G_{1i}, G_{3i}, G_{4i} are given in Eq. (5.10a) and G_{5i} is given in Eq. (II-12).

When $B_{ij} = 0$, the buckling determinant is reduced in size to 2x2 since only the first two boundary conditions of Eq. (II-15) need to be considered.

I.2 Equations for Structural Sections and Stiffened Plates

Equations necessary for the analysis involving plate elements with $B_{ij} = 0$ are complete in the main text. The corresponding equations for the simpler, uncoupled cases of $B_{ij} = 0$ will be given here for reference.

65

Flat plate element-forces and displacements in local coordinates

For the case of $B_{ij} = 0$, the displacement functions assumed are:

$$w = \sum_{i=1}^{4} W_i \, e^{\beta_2} \sin\alpha$$

$$v = \sum_{i=1}^{4} V_i \, e^{\beta_1} \sin\alpha \qquad (II-18)$$

$$u = \sum_{i=1}^{4} U_i \, e^{\beta_1} \cos\alpha$$

where $\alpha(\alpha = m\pi x/a)$ is the same as before. The symbol β used in Eq. (5.18) is changed to β_1 and β_2 in order to distinguish the characteristic roots obtained in bending and in stretching which are now uncoupled. They are defined as:

$$\beta_1 = p_{ui} \pi y/a \qquad (II-19)$$

$$\beta_2 = p_{wi} \pi y/a$$

The displacement functions after satisfying the equilibrium equations (through Eqs. (4.5) and (4.6)) reduce to the determinantal equation of Eq. (5.4) where R_{13}, R_{23}, R_{31} and R_{32} are now zero. This results in two separate equations. The first one is

$$\begin{vmatrix} R_{11} & R_{12} \\ R_{21} & R_{22} \end{vmatrix} = 0 \qquad (II-20)$$

These four elements are the same as in Eq. (5.5) with a replacing b and p_{ui} replacing p_i which, after expansion, becomes

$$K_{u4} p_{ui}^4 + K_{u2} p_{ui}^2 + K_{u0} = 0 \qquad (II-21)$$

which yields four roots of p_{ui} to be used in u and v displacements in Eq. (II-18). V_i in Eq. (II-18) can now be expressed in terms of U_i as:

$$V_i = L_{3i} U_i \qquad (II-22)$$

where

$$L_{3i} = -R_{11}/R_{12} = -R_{21}/R_{22} \qquad (II-23)$$

The second equation is

$$R_{33} = 0 \qquad (II-24)$$

where R_{33} is the same as in Eq. (5.5) with a replacing b and p_{wi} replacing p_i. It is a fourth order polynomial in even powers of p_{wi}. The four values of p_{wi} from Eq. (II-24) are to be used with w displacements in Eq. (II-18).

Using these p_{ui} and p_{wi} values, the three displacements in Eq. (5.13) can be expressed in terms of U_i and W_i as:

$$w = \sum_{i=1}^{4} W_i e^{\beta_2} \sin\alpha = \sum_{i=1}^{4} \omega_{wi} W_i \sin\alpha$$

$$u = \sum_{i=1}^{4} U_i e^{\beta_1} \cos\alpha = \sum_{i=1}^{4} \eta_{ui} U_i \cos\alpha \qquad (II-25)$$

$$v = \sum_{i=1}^{4} U_i L_{3i} e^{\beta_1} \sin\alpha = \sum_{i=1}^{4} \rho_{ui} U_i \sin\alpha$$

and by differentiation,

$$w_{,y} = \sum_{i=1}^{4} W_i(\pi p_{wi}/a)e^{\beta_2} \sin\alpha = \sum_{i=1}^{4} \phi_{wi} W_i \sin\alpha \qquad (II-26)$$

Using the above displacements, the four stress resultants in Eq. (5.12) can be written as (through Eqs. (4.5) and (4.6)):

$$Q_{22} = \sum_{i=1}^{4} \{D_{12}(m/a)^2(p_{wi}/a)-D_{22}(p_{wi}/a)^3+4D_{66}(m/a)^2(p_{wi}/a)\}W_i \pi^3 e^{\beta_2}\sin\alpha$$

$$= \sum_{i=1}^{4} q_{wi}W_i\sin\alpha \qquad (II-27)$$

$$M_{22} = \sum_{i=1}^{4} \{D_{12}(m/a)^2-D_{22}(p_{wi}/a)^2\}W_i \pi^2 e^{\beta_2}\sin\alpha = \sum_{i=1}^{4} (m_{22})_{wi}W_i\sin\alpha \qquad (II-28)$$

$$N_{12} = \sum_{i=1}^{4} \{A_{66}[(p_{ui}/a)+(m/a)L_{3i}]U_i \pi e^{\beta_1}\cos\alpha = \sum_{i=1}^{4} (n_{12})_{ui}U_i\cos\alpha \qquad (II-29)$$

$$N_{22} = \sum_{i=1}^{4} \{-A_{12}(m/a)+A_{22}(p_{ui}/a)L_{3i}\}U_i \pi e^{\beta_1}\sin\alpha = \sum_{i=1}^{4} (n_{22})_{ui}U_i\sin\alpha \qquad (II-30)$$

Transformations to the reference plane
When $B_{ij} = 0$, corresponding to Eqs. (5.23), one has

$$w_s = \sum_{i=1}^{4} (\omega_{wi} + y_o\phi_{wi})W_i \sin\alpha \qquad (II-31)$$

67

$$w_{s,y} = \sum_{i=1}^{4} \phi_{wi} W_i \sin\alpha \tag{II-32}$$

$$u_s = \sum_{i=1}^{4} [n_{ui}U_i - z_o(m\pi/a)\omega_{wi}W_i + y_o(\pi p_{ui}/a)n_{ui}U_i]\cos\alpha \tag{II-33}$$

$$v_s = \sum_{i=1}^{4} (\rho_{ui}U_i - z_o\phi_{wi}W_i)\sin\alpha \tag{II-34}$$

Or written in matrix form

$$\left\{ \begin{array}{c} w_s \\ w_{s,y} \\ u_s \\ v_s \end{array} \right\} = \left[\begin{array}{c} X_1^* \\ (4\times8) \end{array} \right] \left\{ \begin{array}{c} W_1 \\ \vdots \\ W_4 \\ U_1 \\ \vdots \\ U_4 \end{array} \right\} \tag{II-35}$$

i.e. $\quad \{d_{PS}\} = [X_1^*] \{R_1^*\} \tag{II-36}$

$\{R_1^*\}$ is self-evident.

The boundary forces, for $B_{ij} = 0$, are

$$(Q_{22})_s = \sum_{i=1}^{4} [q_{wi}W_i + z_o(n_{12})_{ui}(m\pi/a)U_i]\sin\alpha \tag{II-37}$$

$$(M_{22})_s = \sum_{i=1}^{4} [(m_{22})_{wi}W_i + y_o q_{wi}W_i - z_o(n_{22})_{ui}U_i]\sin\alpha \tag{II-38}$$

$$(N_{12})_s = \sum_{i=1}^{4} (n_{12})_{ui}U_i\cos\alpha \tag{II-39}$$

$$(N_{22})_s = \sum_{i=1}^{4} [(n_{22})_{ui} + y_o(n_{12})_{ui}(m\pi/a)]U_i\sin\alpha \tag{II-40}$$

Or written in matrix form:

$$\left\{ \begin{array}{c} (Q_{22})_s \\ (M_{22})_s \\ (N_{12})_s \\ (N_{22})_s \end{array} \right\} = \left[\begin{array}{c} X_2^* \\ (4\times8) \end{array} \right] \left\{ \begin{array}{c} W_1 \\ \vdots \\ W_4 \\ U_1 \\ \vdots \\ U_4 \end{array} \right\} \tag{II-41}$$

68

i.e.

$$\{f_{PS}\} = [X_2^*] \{R_1^*\} \qquad\qquad (II\text{-}42)$$

Flat-plate element - forces and displacements in global coordinates
For $B_{ij} = 0$, equations similar to Eqs. (5.33), (5.34), (5.36), and (5.37) are

$$\{d_{PG}^+\} = [T_d] [X_1^{*+}] \{R_1^*\} = [X_3^{*+}] \{R_1^*\} \qquad y = +b/2 \qquad (II\text{-}43)$$

$$\{d_{PG}^-\} = [T_d] [X_1^{*-}] \{R_1^*\} = [X_3^{*-}] \{R_1^*\} \qquad y = -b/2 \qquad (II\text{-}44)$$

$$\{f_{PG}^+\} = [T_f] [X_2^{*+}] \{R_1^*\} = [X_4^{*+}] \{R_1^*\} \qquad y = +b/2 \qquad (II\text{-}45)$$

$$\{f_{PG}^-\} = [T_f] [X_2^{*-}] \{R_1^*\} = [X_4^{*-}] \{R_1^*\} \qquad y = -b/2 \qquad (II\text{-}46)$$

where the matrix $[X_3^{*+}]$ is the matrix $[X_3^*]$ with its y replaced by +b/2, etc.

The equations for a plate element in global coordinates are complete with the addition of Eqs. (II-43 to 46) which will be used for a plate element when its $B_{ij} = 0$. In such case, one simply uses $\{R_1^*\}$, $[X_3^{*+}]$, $[X_3^{*-}]$, $[X_4^{*+}]$ and $[X_4^{*-}]$ to replace $\{R_1\}$, $[X_3^+]$, $[X_3^-]$, $[X_4^+]$, and $[X_4^-]$ respectively.

The boundary conditions corresponding to a plate element with $B_{ij} = 0$ can be easily derived from the above equations and will not be presented here.

2. ADDITIONAL ANALYTICAL CORRELATIONS

Two more correlations of the present method with analytical results from existing literature will be given here.

2.1 Buckling of an Angle Section (Ref. II-1)

Figure II.1 shows the buckling load of a column, its cross section is an angle. Curves A and B are results taken from Ref. II-1. The former is obtained by assuming that the angle is made of two plates, each one is simply supported at three sides and the fourth side is free. Correlation with the present method is good even though the three-sides-simply-supported assumption does not satisfy exactly the continuity conditions along the common boundary of the two plate elements. The second curve, B, which treats the column as an Euler column with pin ends, is almost one-half the value obtained by the present method which assumes a line support at the ends with simple support conditions rather than a pin-end phenomenon. Considering that an Euler column with clamped ends has a buckling load four times the value of its pin-ended counterpart, the result from the present method which is about twice the pin-ended column solution seems reasonable.

2.2 Buckling of Beaded or Lipped Isotropic Sections and Plates (Refs. 9, II-2, 19, 22)

Geometries of some isotropic sections and plates with beads, flanges and lips are shown in Fig. II-2. These structures and the corresponding analytical results of buckling are taken from Refs. 9, II-2, 19 and 22 where beads and

lips are treated as beams. The major difference between the present method and these references is the omission of continuities in in-plane displacements at common boundaries and neglect offset between plate and beam elements in these references. Table II.1 shows the results of correlations which seem to be reasonably good.

Table II.1 Correlation of beaded or lipped
isotropic sections and plates

Section	Shown in figure II-2	Buckling Load, $\overline{N}_{11}$, lb/in., on the plate element without including load on stiffener			
		From reference		Present Method	Ratio
		Buckling load	Ref. No.		
Beaded plate	-a	12,280 (m=1)*	II-2	11,403 (1)	1.07
Beaded plate	-b	96	19	94 (1)	1.02
Flanged plate (simple support)	-c	862 (1)	9	907 (1)	0.95
Flanged plate (clamped)	-d	1,840 (1)	9	1,853 (1)	0.99
Flanged plate	-e	19,600 (1)	II-2	18,899 (1)	1.04
Lipped channel	-f	1,030	22	1,138 (10)	0.91
Lipped Z-section	-g	1,030	22	1,137 (10)	0.91

* m = axial half-wave number

3. Geometry of Boeing Test Specimens of Composite Plates

In Section (7, B) of the main text, the results of correlations between tests of Boeing specimens of composite plates and the analytical predictions were given in Table 7.3. The geometry of these specimens are given here in Table II.2.

70

Table II.2 Composite Plate Thickness Data (Boeing)

Plate Specimen	Layer Thickness and Total Thickness	Layer Thicknesses (inch)		
		Specimen (-1)	Specimen (-2)	Specimen (-3)
8A	Titanium	.0195	.0195	.0195
	Adhesive	.0185	.0195	.0125
	Composite	.0650	.0650	.0650
	Total	.103	.104	.097
8B	Titanium	.0317	.0317	.0317
	Adhesive	.0166	.0176	.0156
	Composite	.0557	.0557	.0557
	Total	.104	.105	.103
8C	Titanium	.0340	.0340	.0340
	Adhesive	.020	.019	.019
	Composite	.0470	.0470	.0470
	Total	.101	.100	.100
8D	Titanium	.0504	.0504	.0504
	Adhesive	.0171	.0181	.0181
	Composite	.0375	.0375	.0375
	Total	.105	.106	.106
8E	Composite	.0332	.0332	.0332
	Adhesive	.0107	.0122	.0122
	Titanium	.0232	.0232	.0232
	Adhesive	.0107	.0122	.0122
	Composite	.0332	.0332	.0332
	Total	.111	.114	.114
8F	Composite	.0274	.0274	.0274
	Adhesive	.01825	.01625	.01575
	Titanium	.0327	.0327	.0327
	Adhesive	.01825	.01625	.01575
	Composite	.0274	.0274	.0274
	Total	.124	.120	.119
8G	Composite	.0232	.0232	.0232
	Adhesive	.02055	.01955	.01605
	Titanium	.0395	.0395	.0395
	Adhesive	.02055	.01955	.01605
	Composite	.0232	.0232	.0232
	Total	.127	.125	.118

8H	Composite	.0168	.0168	.0168
	Adhesive	.0127	.0147	.0132
	Titanium	.0530	.0530	.0530
	Adhesive	.0127	.0147	.0132
	Composite	.0168	.0168	.0168
	Total	.112	.116	.113

4. Determination of Buckling Load by Southwell Plot

As mentioned in the main text, in some cases of the buckling test of composite plate specimens which results are given in Table 7.3, it is difficult to determine the buckling load from a load-deflection curve. Some of the buckling loads are obtained by the Southwell plot. Two of such plots are shown in Figures II.3 and II.4 for reference. In Figure II.3, the Southwell plot helped to decide that buckling occurred at a higher large-deflection point rather than at a lower value in the longitudinal load-deflection curve. In Figure II.4, the plot helped to determine the buckling load in the longitudinal load-deflection curve which seemed to have no noticeable buckling point.

References for the Appendix

II-1 Timoshenko, S. P., and Gere, J. M., "Theory of Elastic Stability," 2nd Ed., 1961, McGraw-Hill Book Company.

II-2 Goodman, S., "Elastic Buckling of Outstanding Flanges Clamped at ONe Edge and Reinforced by Bulbs at the Other," TN-1958, October 1949, NACA, Table 2, p. 8.
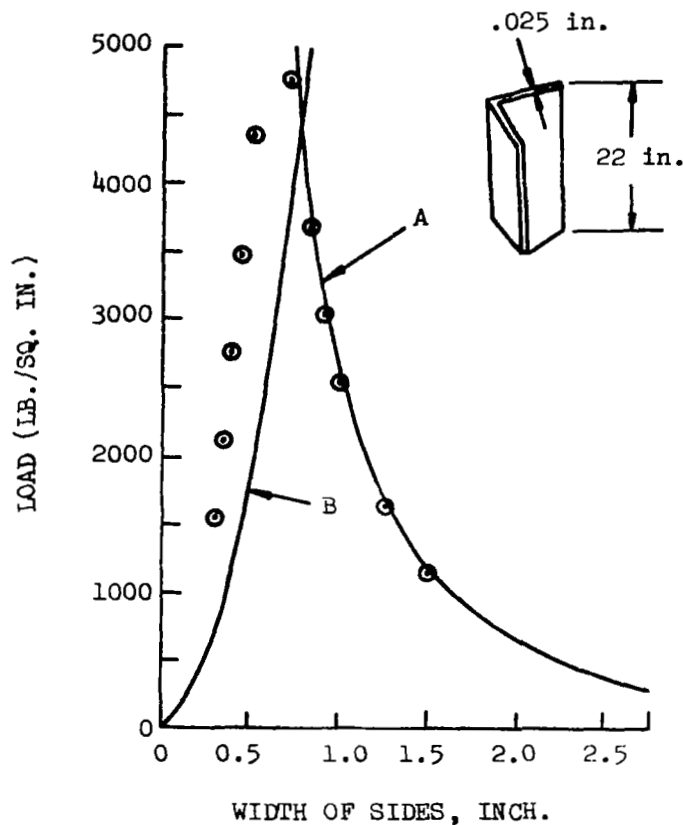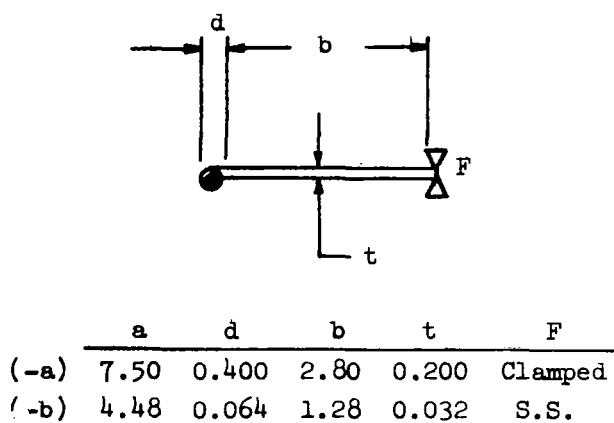
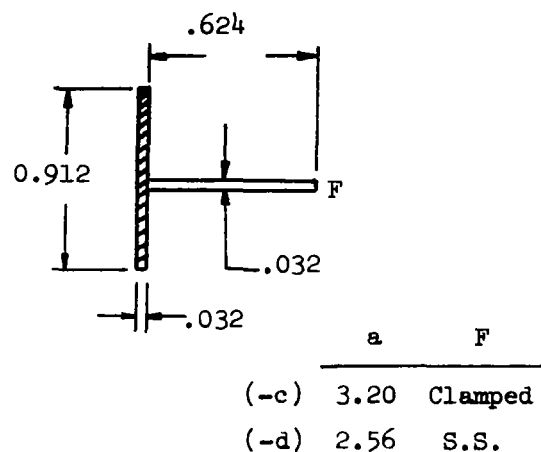Fig. II.1 Buckling of angle section (Ref. II-1)

Curve A: Theoretical curve from Ref. II-1 for buckling of section treated as two separate plate elements and each one is simply supported at three sides and the fourth side free.

Curve B: Theoretical curve from Ref. II-1 for buckling of section treated as an Euler column with the ends hinged.
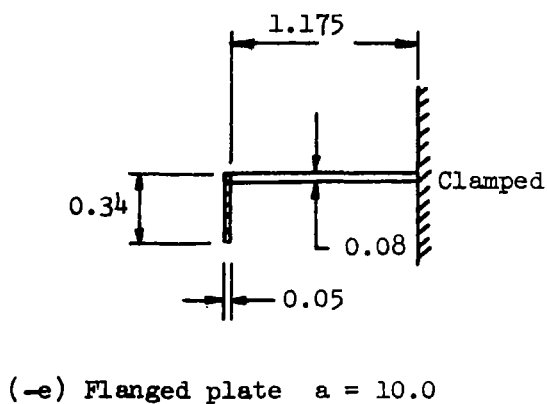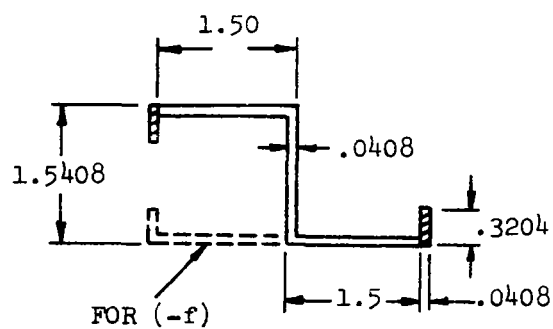
⊙   From the present analysis

	a	d	b	t	F
(-a)	7.50	0.400	2.80	0.200	Clamped
(-b)	4.48	0.064	1.28	0.032	S.S.

Beaded plate

	a	F
(-c)	3.20	Clamped
(-d)	2.56	S.S.

Flanged plate

(-e) Flanged plate   a = 10.0

(-f) Lipped channel   a = 15.0

(-g) Lipped Zee-section a = 15.0

Fig. II.2   Geometry of sections with isotropic beads and lips
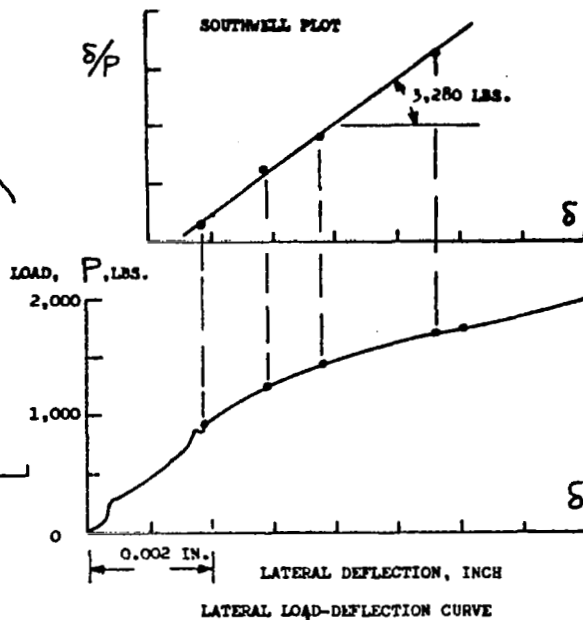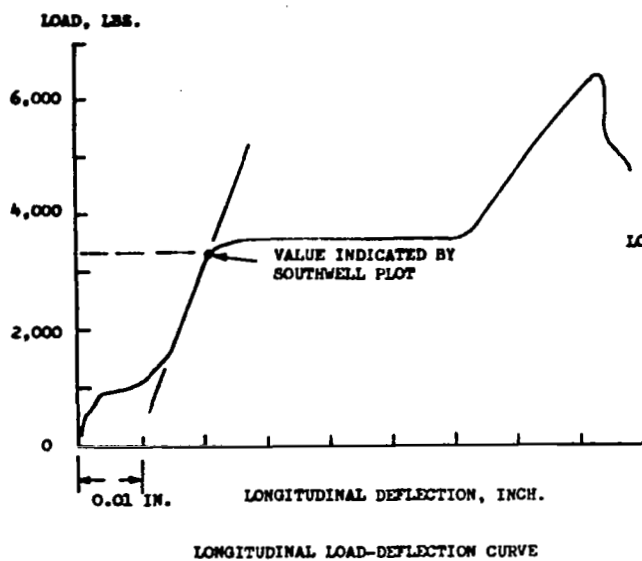a = length of specimen

Fig. II-3 Longitudinal and lateral load-deflection curves of flat plate test specimen 8G No. 2 (Clamp-clamp-free-free case) and the Southwell plot
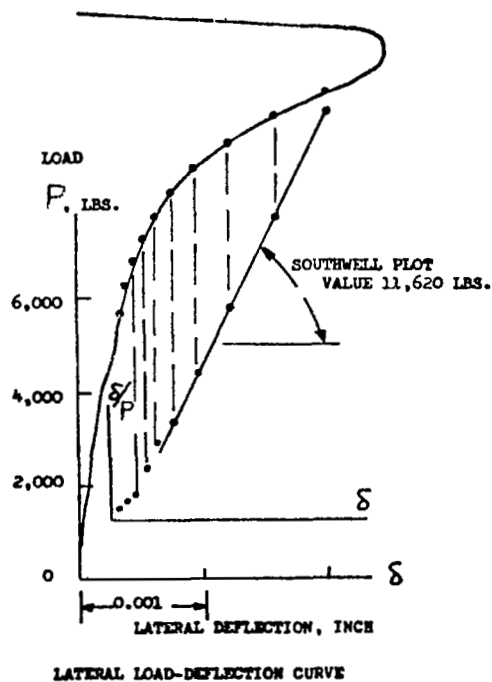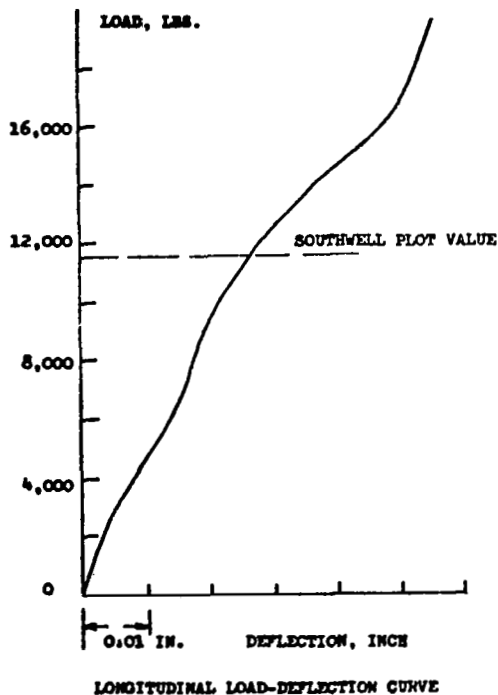

Fig. II-4 Longitudinal and lateral load-deflection curves of flat plate test specimen 8A No. 1 (Clamp-clamp-simple-simple case) and the Southwell plot